Volcanic Glasses at the Izu Arc Volcanic Front: New Perspectives on Fluid and Sediment Melt Recycling in Subduction Zones

Geochemistry Geophysics Geosystems G3
AN ELECTRONIC JOURNAL OF THE EARTH SCIENCES
Published by AGU and the Geochemical Society

Article
Volume 5, Number 1
22 January 2004
Q01007, doi:10.1029/2002GC000408
ISSN: 1525-2027

Volcanic glasses at the Izu arc volcanic front: New perspectives on fluid and sediment melt recycling in subduction zones

S. M. Straub
GEOMAR Forschungszentrum an der Christian-Albrechts Universität zu Kiel, Wischhofstrasse 1-3, 24148 Kiel, Germany

Now at Lamont Doherty Earth Observatory of Columbia University, 61 Route 9W, Palisades, New York 10964, USA (smstraub@ldeo.columbia.edu)

G. D. Layne
Woods Hole Oceanographic Institution, MS 23, Clark 114A, Woods Hole, Massachusetts 02543, USA

A. Schmidt
GEOMAR Forschungszentrum an der Christian-Albrechts Universität zu Kiel, Wischhofstrasse 1-3, 24148 Kiel, Germany

C. H. Langmuir
Lamont Doherty Earth Observatory of Columbia University, 61 Route 9W, Palisades, New York 10964, USA

Now at Department of Earth and Planetary Sciences, Harvard University, 20 Oxford Street, Cambridge, Massachusetts 02138, USA

[1] Volcanic glasses contained in distal fallout tephras from the Izu arc volcanic front (Izu VF) provide unique perspectives on general problems of arc volcanism. Unlike cogenetic lavas, these glasses are liquid compositions where element concentrations as well as ratios have significance. Isotopic evidence and previous work show that there is no sediment melt contribution to the sources of the Izu VF tephras, and hence their trace element characteristics permit determination of the trace element contents of slab fluids. The slab fluid is a composite of metasediment (~5% of total fluid) and metabasalt (~95%) component fluids, and carries large ion lithophile elements (LILE) with high LILE/Th and LILE/U, and low Th and U relative to source. Except for Sr and K, the metabasalt fluid is much less enriched than the metasediment fluid, but its large relative proportions make it an important carrier of many trace elements. The metabasalt fluid has the characteristics of the arc trace element signature, obviating the need for ubiquitous involvement of sediment in arc magma genesis. The fluid component in the tephras is remarkably constant in composition over fifteen million years, and hence appears to be a robust composition that may be applicable to other convergent margins. Assuming that the metabasalt fluid is a common component, and that distribution coefficients between sediment and fluid are similar from one arc to another, composite fluid compositions can be estimated for other arcs. Differences from this composition then would likely result from a sediment melt component. Comparison to arcs with sediment melt components in their source (Marianas, eastern Aleutians) shows that partial sediment melts may be so enriched, that they can completely mask the signature of the comingling slab fluids. Hence sediment melts can easily dominate the trace element and isotopic signature of many convergent margins. Since sediment melts inherit the LILE/LILE ratios of the trench sediment, Earth's surface processes must eventually influence the compositional diversity of arcs.

Components: 21,038 words, 21 figures, 9 tables.

Keywords: Volcanic arcs; slab fluids and melts; recycling; Izu Bonin.

Index Terms: 1030 Geochemistry: Geochemical cycles (0330); 1065 Geochemistry: Trace elements (3670); 8404 Volcanology: Ash deposits.

Received 16 July 2002; **Revised** 7 November 2003; **Accepted** 13 November 2003; **Published** 22 January 2004.

Straub, S. M., G. D. Layne, A. Schmidt, and C. H. Langmuir (2004), Volcanic glasses at the Izu arc volcanic front: New perspectives on fluid and sediment melt recycling in subduction zones, *Geochem. Geophys. Geosyst.*, *5*, Q01007, doi:10.1029/2002GC000408.

1. Introduction

[2] Igneous petrogenesis relies largely on the production and subsequent evolution of liquids created through partial melting and differentiation. Direct measurement of liquid compositions are possible through volcanic glasses. Indeed, glass compositions have been invaluable in developing a quantitative understanding of ocean ridge basalts. At convergent margins, however, volcanic glasses are exceedingly rare. Consequently, virtually all chemical analyses are made on whole rock compositions, where variable and usually unknown proportions of phenocrysts modify the chemical abundances. It is for this reason that preserved melt inclusions have such value, but their compositions also often reflect complex processes and post-entrapment modification that make them more difficult to interpret. In this study we report on volcanic glass compositions recovered from sediment cores outboard of the Izu Volcanic arc. Like the study of *Bryant et al.* [1999], and in contrast to other suites of arc volcanic rocks, these glass analyses provide true liquid compositions, and therefore both elemental abundances and elemental ratios have primary petrogenetic significance.

[3] Glass compositions permit a more reliable approach to the quantification of recycling processes at convergent margins. A particularly elusive variable of the flux equation is the composition of individual fluid and melt components that are added from the slab to a mantle source. Slab fluids, identifiable by their ^{238}U excesses, originate from sedimentary and basaltic source rocks, and presumably have the typical trace element patterns of arc lavas [e.g., *Tatsumi et al.*, 1986; *Brenan et al.*, 1995a, 1995b; *Kogiso et al.*, 1997; *Johnson and Plank*, 1999; *Turner et al.*, 2000; *Sigmarsson et al.*, 2002]. On the other hand, enrichments of elements that are not mobilized by fluids (e.g., Th, Nb, Ta, REE) suggest the presence of partial slab melts of subducted sediments in the source [e.g., *Elliott et al.*, 1997; *Class et al.*, 2000]. The subducted sediment often already possesses the arc-like signature of the upper continental crust and, if not fractionated during partial melting, will transmit this signature to arcs [*Plank and Langmuir*, 1998; *Morris et al.*, 1990; *Plank and Langmuir*, 1993].

[4] A straightforward way to distinguish among these components in arc sources is to determine their full trace element composition. However, to date, attempts determining element concentrations have often come to differing conclusions [e.g., *Class et al.*, 2000; *Hochstaedter et al.*, 2001]). Forward modeling procedures remain uncertain because of the paucity of reliable experimental data on solid/fluid and solid/melt partitioning, and the uncertainties of the residual mineralogy of the slab at the relevant slab depths (e.g., amphibolite versus eclogite; *Tatsumi and Kosigo* [1997]; *Johnson and Plank* [1999]; *Patino et al.* [2000]). The inverse approach, i.e., the interpretation of the observed geochemistry of the arc magmas, is impaired if several slab components (fluids, melts) comingle in the arc source [e.g., *Elliott et al.*, 1997; *Class et al.*, 2000]. The inverse approach can be strengthened by using glass compositions in arc settings where the slab-derived components are spatially resolved, and

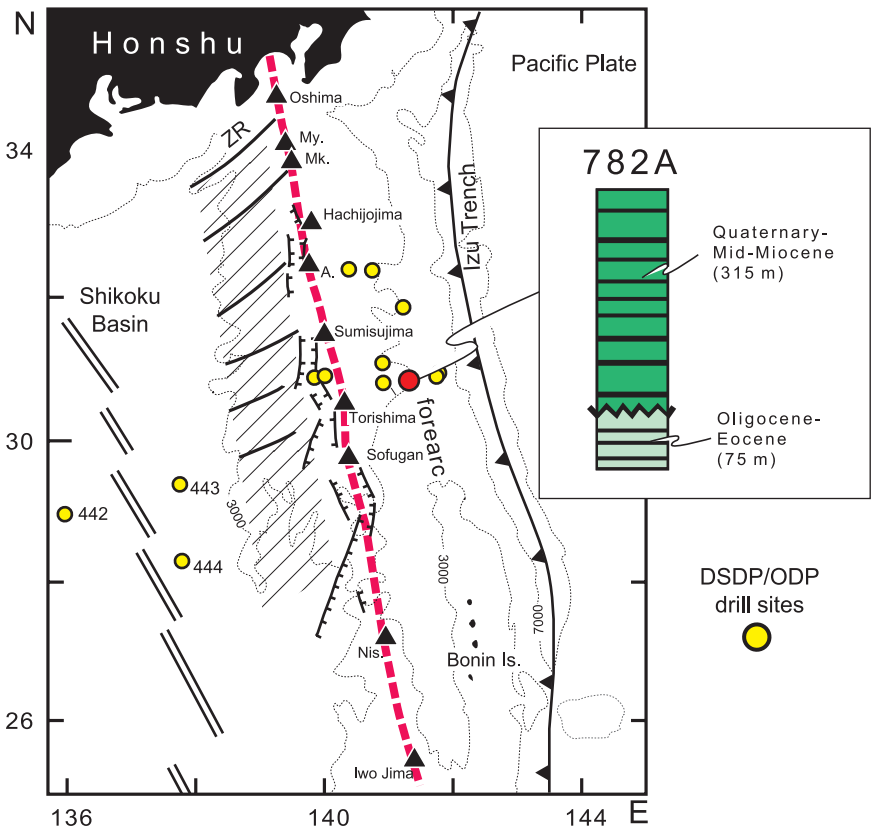

Figure 1. Geological setting of the Izu-Bonin arc/backarc system with DSDP and ODP drill sites. From East to West: Pacific Plate, Izu Trench, Izu Fore-arc, Izu Volcanic Front (red stippled line), rift (grabens), Rear-arc (hatched) and inactive Shikoku Backarc Basin. Depth contours are in meters. ZR, Zenisu Ridge; subaerial volcanoes (black triangles) unless otherwise indicated are My, Miyakejima; Mk, Mikurajima; A, Aogashima; Nis, Nishinoshima. BI, Bonin Islands (uplifted Eocene fore-arc basement). Diagonal solid lines in rear-arc region indicate the preferred alignment of rear-arc volcanoes (across-arc chains). Stratigraphy of Site 782A after *Xu and Wise* [1992].

where the effects of crustal contamination and background mantle enrichment are negligible.

[5] Thus a confluence of favorable characteristics to address the issues of subduction components occurs in the central Izu arc, a thin-crusted (~20 km) intraoceanic volcanic arc in the Northwest Pacific (Figure 1). Below the volcanic front (Izu VF), the mantle is fluxed by slab-derived aqueous fluids only, originating from both the metabasalt and metasediment layers of the subducting slab [*Taylor and Nesbitt*, 1998; *Hochstaedter et al.*, 2001]. The Izu VF background mantle is both well defined and highly depleted in high-field-strength elements (HFSE) and rare earth elements (REE), having low $(La/Sm)_n$ ratios (~0.9 ± 0.2), and radiogenic Nd isotopes similar to the most radiogenic Indian MORB. The low concentrations mean that for most elements the mantle wedge makes a negligible contribution to the element budgets. Therefore the Izu VF should be well suited for characterizing the slab fluid flux, in contrast to arc settings that have unambiguous partial sediment melt components in their source (e.g., Marianas, eastern Aleutians). Lastly, unique perspectives on the Izu VF are provided by volcanic glass particles from tephra fallout layers, that record true liquid compositions as well as possible variations through time.

2. Geological Setting, Sample, and Methods

2.1. Geological Setting

[6] The evolution of the intraoceanic Izu Bonin arc/backarc system in the NW Pacific began in the middle Eocene at ~49 Ma following the subduction of the Pacific plate beneath the Philippine

plate in westerly direction (see *Taylor* [1992] and *Hochstaedter et al.* [2001] for detailed description). In the Oligocene (~31 Ma) the Izu arc split alongstrike and during the Miocene, the interarc rift developed into the Shikoku backarc spreading center. Volcanism at the Izu VF waned during backarc spreading (~24 to 15 Ma), but rejuvenated ~15 Ma ago, and has been vigorous since. A new period of intraarc rifting was initiated at ~2.8 Ma immediately west of the Izu VF (Figure 1). The Quaternary Izu VF is constructed on ~20 km thick crust [*Suheyiro et al.*, 1996], and located about ~100 km above a well-defined Wadati-Benioff zone [*Katsumata and Sykes*, 1969]. The subducting slab is composed of Jurassic basaltic crust (~132 Ma) similar in composition to the mid-ocean ridge basalts of the East Pacific Rise [*Plank et al.*, 2000]. The basaltic crust is covered by ~400 m thick Mesozoic and Cenozoic pelagic sediment [*Plank et al.*, 2000] consisting of clay (~39%), arc-derived ash (~5%) and a mixture of chert, nannofossil chalk and marls (~56%) [*Plank et al.*, 2000].

[7] The Neogene Izu arc has a broad volcanic zone (~200 km) [*Hochstaedter et al.*, 2000, 2001] and a shallow-dipping slab (~45–50° [*Hilst and Seno*, 1993]). Geochemical transects confirm the presence of slab components in the mantle sources across the entire width of the arc [*Taylor and Nesbitt*, 1998; *Hochstaedter et al.*, 2001]. While there is agreement on an exclusively fluid contribution to the volcanic front, the exact nature of the slab components behind the volcanic front (=rear-arc) is currently in debate. *Hochstaedter et al.* [2001] proposed the existence of slab fluids, in contrast to the mixture of partial slab melts and fluids suggested by *Schmidt et al.* [1999] and *Plank and Kelley* [2001].

2.2. Izu Tephra Samples

[8] The tephra fallout was recovered in the mid-Miocene to Quaternary sediments drilled on the outer Izu fore-arc at ODP Site 782A (30°51.66′N, 141°18.85′E), located ~120 km east of the Quaternary arc volcanic front (Figure 1). At this site, 330 m of Neogene sediment consists of nannofossil chalk that is interspersed by centimeter - thick brown to blackish, and rarely, light-colored tephra fallout. There is no evidence for significant disturbance of the stratigraphic sequence by bioturbation, and hence each tephra fallout layer represents a single eruption event. A total of 111 discrete tephra layers were deposited in the mid-Miocene to Quaternary sediments. Given a recovery rate of 59%, this corresponds to a minimum of seven to eight major eruptions per one million years [*Fryer et al.*, 1992; *Xu and Wise*, 1992].

[9] The fallout tephra is composed of ash-sized (<2 millimeter) lithic, vitric and mineral particles, and subordinate biogenic material. In most tephras, lithic particles and phenocrysts are far more abundant than glass shards, although pristine glasses are well distributed throughout the Neogene. Volcanic glass shards range from brown vesicle-poor sideromelane to vesicle-rich glass and frothy pumice. In some layers, volcanic glass is confined to the melt inclusions of the phenocrysts. Pristine glasses are identified from the absence of any signs of birefringence under crossed polarizers. The absence of alteration is further confirmed by the distribution of alteration-sensitive elements (e.g., Cl, B, δ^{11}B, Li) and the compositional similarity of matrix shards and melt inclusions [e.g., *Straub and Layne*, 2002]). Common phenocrysts are; intermediate and calcic plagioclase (An_{42-96}), clinopyroxene (En_{34-75}) and orthopyroxene (En_{41-73}). However, olivine and amphibole were never observed. Titanomagnetite (Usp_{14-50}) is common except in the basaltic tephras. Cl-rich apatite (Cl = 0.8–2.4 wt%) (common) and quartz (very rare) are trace phases in dacitic and rhyolitic tephras only.

2.3. Sample Preparation and Analytical Methods

2.3.1. Sample Preparation and Selection

[10] A volume of 5 to 10 cubic centimeters of each tephra sample was freeze-dried and wet-sieved through a 32 μm polyester screen using de-mineralized water. Glass particles were handpicked under a binocular microscope. The glass shards were mounted in a distinctive pattern that enabled mapping and retracing of individual shards for multiple analyses. The samples were ground on sanding

paper until the exposure of a suitable cross-section and finished by polishing on diamond (6 micron) and alumina (1 micron and 0.5 micron) suspensions. On the basis of a pilot study (Straub 2003), and petrographic examination, 18 fallout tephra with large, clear, pristine glass shards were selected for this study. These tephras range from 1.9 to 14.2 million years in age (Table 1). Approximately 15 individual glasses per fallout tephra were analyzed for the major elements by electron microprobe. Fourteen tephra samples that contained basaltic to rhyolitic glasses were selected for the ion probe analyses of B and Li (2 to 8 glasses per sample). A subset of seven samples with large, clear and vesicle- and crystal-poor glass shards were analyzed by laser ablation ICP-MS (3 to 4 glasses per sample). The data are presented in Table 1.

2.3.2. Electron Microprobe

[11] Electron microprobe analyses were carried out at the GEOMAR Research Center (Kiel/F.R.G.) by means of a SX50 Cameca electron microprobe analyzer equipped with four wavelength dispersive spectrometers. Samples were carbon-coated prior to analyses. The elements Si, Ti, Al, Mn, Fe, Mg, Ca and Na were analyzed at 15 keV acceleration voltage with a defocused beam of 20 micrometer. The beam current was at 4 nA for Si and Na; all other elements were analyzed at 10 nA. Peak counting times ranged from 10 sec (Na) to 60 seconds. K and P were analyzed in the Cameca trace mode at 10 keV, 30 nA beam current, 10–20 micrometer beam diameters and 60 sec (K) and 100 sec (P) peak counting times. A ZAF data reduction was carried out by means of the in-built PAP routine. All elements were corrected for instrument drift by normalizing to the same chip of basalt glass JDF-D2 (wt% oxides: SiO_2 = 50.8, TiO_2 = 1.93, Al_2O_3 = 13.8, FeO* = 12.17, MnO = 0.22, CaO = 10.8; Na_2O = 2.77; K_2O = 0.215; P_2O_5 = 0.23). Precision and accuracy of analyses are given in Table 2.

2.3.3. Secondary Ion Mass Spectrometry (SIMS)

[12] Boron and lithium concentrations were determined by SIMS using the Cameca IMS 3f ion microprobe at Woods Hole Oceanographic Institution. The carbon coating used for electron microprobe analysis was removed, and the samples cleaned, by gently rubbing with an alcohol-soaked cloth. The samples were then dried with an ultrafiltered dust blower before sputter- coating with 300 Angstrom of Au. The ion probe was operated at a nominal 8 keV primary accelerating voltage with $^{16}O^-$ primary beam and a mass resolution of 300. The primary beam current was 30–40 nA. Secondary ions were extracted through a nominal accelerating potential of 4500 eV. Extraneous secondary ions were excluded by a 68 micrometer field aperture. Isobaric interferences were effectively eliminated with a 40 eV energy window and sample offset voltage of −50 eV. Each analysis location was precleaned by rastering the primary beam over a 70 micrometer square for 4 minutes. A focused, 20–30 micrometer diameter spot beam of was then re-centered on spot for two more minutes before collecting counts. B was calibrated by means of four glasses of variable silica content (JDF-D2, NIST 610, NIST 612, UTR-2; Table 3). The average secondary ion yield of B normalized to Si (i.e., $(B^+/Si^+)/(B/Si)$) was 0.487 ± 0.055 in the measurement period (December 1997 to October 1998), comparable to that reported by *Gurenko and Chaussidon* [1997] for the CRPG-Nancy IMS 3f instrument (0.474 ± 0.043). This implies a minimum accuracy of 11% relative. For B, any additional effects from variation of the major element matrix of individual samples (<5% relative) are within this error. The reproducibility of B was determined by repeat measurements on both high-B and low-B glasses, and is better than 10% at B <10 ppm, and better than 5% at higher B contents. Li was calibrated by means of a low-silica glass (JDF-D2) and a high-silica glass (UTR-2), which differ by 60% in the normalized Li secondary ion yield (JDF-D2 = 1.065 ± 0.056; UTR-2 = 1.708 ± 0.062) (Table 3). The Li concentration of samples was calculated using a two-point calibration, and applying a linear correction for the ion yield based on SiO_2 contents. A reproducibility of 4% (relative) for Li was determined on basaltic glass 21DS5 (Li = 5.63 ± 0.22 ppm).

2.3.4. Laser Ablation Analyses

[13] Elements Rb, Sr, Y, Zr, Nb, Cs, Ba, La, Ce, Pr, Nd, Sm, Eu, Gd, Tb, Dy, Ho, Er, Tm, Yb, Lu, Hf,

Table 1 (Representative Sample). Electron Microprobe (Major Elements), Ion Probe (B, Li, Be) and Laser Ablation-ICP-MS Analyses of Individual Glass Shards From Site 782A Tephra Fallout[a] (The full Table 1 is available in the HTML version of this article at http://www.g-cubed.org)

Sample No.	782A-11X-3-0-1			782A-15X-3-9-10			782A-23X-4-107-109			782A-26X-4-52-54			782A-26X-5-147-149				782A-32X-2-26-28		
Glass shard	.19-2	.19-3	.19-9	29-b1	29-c1	29-d2	59-b1	59-d1	59-g1	69-b3/e1	69-e2	69-f1	71-b1	71-e1	71-f3	71-e2	90-c3/d3	90-e2	90-e4
Age (Ma)	2.84	2.84	2.84	3.78	3.78	3.78	8.59	8.59	8.59	10.3	10.3	10.3	10.45	10.45	10.45	10.45	13.35	13.35	13.35
SiO_2	53.16	52.8	53.93	52.28	52.49	51.76	52.5	51.72	52.06	71.95	72.32	75	55.07	56.98	59.72	65.84	65.19	65.17	64.46
TiO_2	1.1	1.1	1.07	1.26	1.26	1.26	1.22	1.21	1.23	0.73	0.7	0.43	1.26	1.14	1.01	0.67	0.74	0.78	0.84
Al_2O_3	15.05	15.07	15.07	14.63	14.89	14.71	14.27	14.05	13.98	13.63	13.41	12.86	15.7	15.28	14.91	13.4	13.62	13.6	14.16
FeO*	12.31	12.17	12.02	12.96	13.23	13.91	13.61	13.59	13.79	3.89	3.76	2.44	10.67	9.51	8.69	4.94	7.91	8.21	8.51
MnO	0.22	0.23	0.26	0.19	0.22	0.25	0.24	0.26	0.23	0.21	0.18	0.19	0.28	0.24	0.22	0.19	0.18	0.2	0.19
MgO	4.2	4.32	4.13	4.48	4.6	4.71	4.95	4.99	4.91	0.88	0.76	0.42	3.97	3.46	3.12	1.49	1.17	1.16	1.53
CaO	8.9	9.03	8.84	9.22	9.38	9.46	9.5	9.53	9.53	3.42	3.24	2.42	8.47	7.62	7.05	4.25	4.82	4.83	5.47
Na_2O	2.76	2.59	2.66	2.34	2.3	2.21	2.21	2.19	2.2	4.45	4.37	4.49	2.72	2.82	2.96	3.91	3.63	3.62	3.52
K_2O	0.22	0.2	0.22	0.38	0.4	0.34	0.34	0.34	0.33	0.65	0.65	0.73	0.24	0.44	0.36	0.6	1.11	1.11	1.04
P_2O_5	0.12	0.13	0.11	0.11	0.1	0.11	0.1	0.1	0.11	0.15	0.16	0.06	0.21	0.16	0.18	0.11	0.14	0.13	0.14
Total	97.91	97.54	98.2	97.74	98.75	98.6	98.83	97.9	98.31	99.8	99.38	98.98	98.4	97.38	97.83	95.28	98.37	98.67	99.72
B*	10	10	10	22	24	24	18	18	18	23	24	27	12	15	15	25	51	50	48
Li*	3.9	4	4	6.7	7	7.3	7.1	7	7	9	8.8	9.3	5.1	6.6	6.1	9.8	14.1	13.9	13.1
Be*	0.57	0.5	0.41	0.48	0.52	0.52	0.42	0.41	0.38	0.66	0.68	0.68	0.47	0.52	0.61	0.66	0.56	0.55	0.53
Cs	0.19	0.17	0.19	0.51	0.51	0.49	0.47	0.47	0.49	0.54	0.59	0.66	0.29	0.41	0.38	0.76	1.33	1.57	1.47
Rb	2.22	2.04	2.17	4.72	5.01	4.85	4.72	4.65	4.75	7.16	7.94	8.9	3.55	4.88	5.48	8.76	14.96	17.76	16.7
Ba	34.5	32.4	34.5	54.5	56.4	55.4	71.4	70.9	71.9	124.8	128.5	144.1	56	70.61	73.37	120.6	160.6	189.6	178.6
Th	0.1	0.08	0.1	0.11	0.11	0.11	0.15	0.12	0.13	0.35	0.35	0.38	0.17	0.21	0.23	0.38	0.48	0.56	0.52
U	0.08	0.07	0.08	0.1	0.11	0.1	0.1	0.09	0.1	0.27	0.25	0.29	0.13	0.17	0.2	0.23	0.29	0.35	0.31
Nb	0.27	0.24	0.25	0.26	0.27	0.27	0.3	0.32	0.3	0.71	0.68	0.69	0.43	0.37	0.54	0.6	0.49	0.59	0.56
Ta	0.023	0.024	0.022	0.024	0.023	0.024	0.022	0.019	0.025	0.051	0.058	0.059	0.047	0.028	0.044	0.061	0.04	0.044	0.044
La	1.44	1.39	1.51	1.64	1.66	1.68	1.69	1.73	1.78	3.87	3.93	4.2	1.86	2.2	2.49	3.42	3.15	3.65	3.43
Ce	4.61	4.33	4.62	5.09	5.16	5.17	5	4.93	4.94	11.92	12.05	12.37	5.69	7.22	7.4	11.28	8.27	9.79	9.22
Pb	1.24	1.12	1.28	2.48	2.52	2.5	2.81	2.79	2.84	3.29	3.38	3.63	1.78	2.22	2.57	3.59	6.63	7.62	7.41
Pr	0.85	0.79	0.84	0.93	0.91	0.93	0.91	0.94	0.91	2.09	2.1	2.15	0.98	1.28	1.37	1.81	1.39	1.62	1.56
Sr	171.2	167.8	170.3	171.5	175.5	175.1	181	179.2	177.2	173.9	165.6	143.3	219	216.2	206.9	182.4	166.5	178.5	186.2
Nd	5.12	4.86	5.21	5.53	5.56	5.46	5.57	5.27	5.52	12.19	11.85	12.15	6.57	7.04	7.27	10.22	7.82	9.07	8.7
Zr	33.3	31.8	34.5	31.8	32.8	32.5	35	34.7	34.5	87.3	89.7	100.4	40.1	50.7	54.9	82.9	59.3	68.8	65.6
Sm	2.06	1.91	2.09	2.09	2.14	2.11	1.95	2.01	2.17	4.37	4.39	4.31	2.54	3.06	2.34	3.53	2.78	3.14	3.18
Hf	1.14	1.09	1.17	1.15	1.2	1.15	1.28	1.27	1.23	3.05	2.98	3.47	1.37	1.73	1.5	2.57	2.05	2.39	2.31
Eu	0.83	0.79	0.85	0.79	0.86	0.85	0.76	0.81	0.79	1.44	1.35	1.25	0.95	0.91	1.06	1.26	0.86	1	0.97
Gd	2.98	2.81	3.07	3.03	2.98	3.21	3.1	3.32	3.16	5.75	5.73	5.49	3.45	3.8	3.97	5	3.93	4.47	4.32
Tb	0.52	0.48	0.53	0.56	0.55	0.55	0.53	0.56	0.54	1.04	1.02	1.02	0.62	0.67	0.64	0.91	0.67	0.8	0.77
Dy	3.99	3.72	3.81	4.07	4.1	4.07	3.95	3.83	3.98	7.64	7.5	7.48	3.96	5.21	4.67	6	5.03	5.79	5.59
Y	21.9	21.4	22.7	22.1	22.6	22.7	23.2	22.8	22.9	43.2	43.3	44.9	23.7	27.7	28.8	38.1	30.1	34.2	33.1
Ho	0.83	0.8	0.87	0.86	0.91	0.9	0.82	0.84	0.88	1.69	1.57	1.66	0.94	1.13	1.11	1.42	1.11	1.25	1.24
Er	2.52	2.36	2.54	2.61	2.63	2.62	2.55	2.47	2.64	4.99	4.88	5.12	2.92	3.16	3.16	4.36	3.35	3.83	3.7
Tm	0.37	0.35	0.38	0.38	0.39	0.38	0.39	0.39	0.39	0.75	0.77	0.79	0.4	0.46	0.52	0.64	0.52	0.59	0.56
Yb	2.58	2.49	2.63	2.62	2.64	2.68	2.54	2.63	2.63	5.43	5.14	5.49	3.03	3.27	3.07	4.25	3.6	4.19	4.07
Lu	0.41	0.37	0.41	0.4	0.42	0.42	0.42	0.38	0.4	0.85	0.81	0.84	0.47	0.46	0.54	0.65	0.55	0.65	0.62

Table 1. (continued)

Sample No.	782A-11X-3-0-1	782A-15X-3-9-10	782A-23X-4-107-109	782A-26X-4-52-54	782A-26X-5-147-149	782A-32X-2-26-28
$^{87}Sr/^{86}Sr$	0.703554	0.703561	0.703513	0.703488	0.703477	0.703605
$^{143}Nd/^{144}Nd$	0.513082	0.513092	0.513074	0.513077	0.513061	0.513078
$^{206}Pb/^{204}Pb$	18.36	18.41	18.44	18.4	18.38	18.38
$^{207}Pb/^{204}Pb$	15.53	15.53	15.53	15.5	15.5	15.52
$^{208}Pb/^{204}Pb$	38.2	38.24	38.29	38.16	38.16	38.25

[a] Numerical ages of tephra are based on calcareous nannofossil stratigraphy [*Xu and Wise*, 1992]. Radiogenic isotopes of Sr, Nd and Pb were determined on handpicked, acid-leached particle separates [*Schmidt*, 2001]. Asterisks, analyzed by ion probe.

Ta, Pb, Th, U were analyzed by laser ablation ICP-MS at the Department of Earth and Planetary Science, Harvard University, Cambridge MA, U.S.A (now at http://www.geol.umd.edu/(~mcdonoug/la-icp-ms.html). The VG Elemental (Winsford, U.K.) Plasma Quad II mass spectrometer was coupled to an Excimer laser (Lambda Physik-Compex 110) with a 193 nm wavelength, a pulse repetition rate of 10 Hz and a pulse energy of ~120 mJ. Laser sampling was done in a He atmosphere using a 100 μm spot size. The intensity data were acquired by peak hopping in pulse counting mode. A total of 150 sweeps was performed for each spot, consisting of a gas blank interval of ~60 sweeps that was followed by the ablation interval (at least 60 sweeps). External calibration was conducted by NIST glass 612 (values of *Pearce et al.* [1997]). All concentrations were corrected by using the previously determined Ca content as internal standard by measuring ^{42}Ca. The data were reduced using the program "LAMTRACE" [*Horn et al.*, 1997]. Data accuracy and precision were monitored by multiple analyses of various reference samples (Table 4). At the relevant levels of abundance, most of the elements measured are within 10% (REE 5%) of the reference value, except for Cs (25%), Rb (12%) and Pb (16%).

2.3.5. Radiogenic Isotopes

[14] Isotopic data (Sr, Nd, Pb) provide an essential complement to the glass data reported here. The isotopic data for these glasses, as well as other samples from Izu arc, have been presented by *Schmidt* [2001] (http://e-diss.uni-kiel.de/diss_465/).

3. Results

3.1. Chemistry of Neogene Izu VF Volcanics

[15] The chemical compositions of the Neogene tephras cover a large range, from 50 wt% to 75 wt% SiO_2 and 0.2 wt% to 1.4 wt% K_2O. The overall low K_2O contents of all the tephras confine them to a low-K magma series, as long established for the Izu VF. The isotope and trace element signatures identify the central Izu arc volcanoes west of Site 782A, and their precursors, as likely sources [e.g.,

Table 2. Precision and Accuracy of Electron Microprobe Analyses[a]

	JDF-D2, n = 8			CFA 47, n = 35			21DS5, n = 49	
	Ref. Value	This Study	s%	Ref. Value	This Study	s%	This Study	s%
SiO_2	50.80	50.75	0.6	61.6	62.3	0.5	50.71	0.6
TiO_2	1.93	1.94	0.7	0.42	0.46	5.4	1.28	1.7
Al_2O_3	13.8	13.73	0.8	18.53	18.74	0.7	17.25	0.6
FeO*	12.17	12.21	0.4	2.65	2.85	3.8	7.78	1.4
MnO	0.22	0.24	7	0.18	0.18	11.3	0.15	15
MgO	6.83	6.85	0.7	0.42	0.44	17.8	7.68	0.8
CaO	10.8	10.8	0.4	1.84	1.86	3.6	11.15	0.6
Na_2O	2.77	2.79	0.7	5.37	5.43	1.2	3.08	1.3
K_2O	0.215	0.22	2.5	7.98	7.92	1.3	0.25	2.3
P_2O_5	0.230	0.23	2.7				0.17	8.9
Total	99.77	99.76		99.71	100.1		99.50	

[a] All data in wt%. JDF-D2 was also used to correct for instrument drift. JDF-D2 is a natural basalt glass from the Juan de Fuca Ridge developed by C. H. Langmuir (Lamont). References values are from personal communication. CFA 47 is a trachytic obsidian from the Phlegrean Fields (Italy) developed by N. Metrich (Gif-sur-Yvette). Reference values are from *Metrich and Clochiatti* [1989]. 21DS5 is a natural basalt glass from the Mariana Trough used to monitor precision. *n* is the number of analyses during the three months measurement period at the Geomar (from September to November 1997). Precision (s%) is reported as the percentage of one standard deviation of *n* repeat analyses of the three reference glasses.

Langmuir et al., 2004; *Taylor and Nesbitt*, 1998; *Hochstaedter et al.*, 2000, 2001]. Despite the fact that the tephras likely originate from several different volcanoes, and 15 Ma years of eruptive history, there is remarkable coherence to their major element variations (Figure 2).

[16] The significant advantage of glass compositions is apparent by comparing major elements of the glasses with published analyses of lavas from the volcanic front lavas (Figure 2). Whereas the lavas occupy large fields of variation, the glass data are largely confined to well-defined one-dimensional arrays that cut across the fields of lava compositions. The tephra glasses have experienced loss of plagioclase, clino- and orthopyroxene, and most likely olivine. Olivine is not present as a phenocryst phase in the tephra, but is common in Izu VF lavas [e.g., *Langmuir et al.*, 2004; *Amma-Miyasaka and Nakagawa*, 2002]. Crystal fractionation is the most likely cause of the limited range of the tephra glasses in major elements at a given MgO, and of the lower CaO and Al_2O_3 relative to the lavas, which contain random contributions from phenocrysts (Figure 2). However, fractional crystallization has not erased all primary signatures in the glasses, as for example the arc-typical Al_2O_3-enrichment of the glasses relative to MORB is maintained (Figure 2) and basaltic andesitic glasses have similar Sr abundances (168–222 ppm; n = 12) as the basaltic andesitic Izu VF lavas (Sr = 161–242 ppm; n = 29). Notably, excluding a single high-MgO basalt (MgO = 8.23 wt%, Mg# 62 [*Taylor and Nesbitt*, 1998]) from Hachijojima volcano, the glasses and Izu VF basalts have similar maximum MgO ~6 wt% and mg# ~60. The tephras extend to far higher SiO_2, no doubt reflecting the fact that silicic compositions largely occur in explosive eruptions that gave rise to tephras. Clearly, the lack of high silica lavas in a particular arc is not necessarily indicative that such silicic tephras are common volcanic products.

[17] Basalt through rhyolitic tephras have similar Sr, Nd, Pb and B isotopic compositions [*Schmidt*, 2001; *Straub and Layne*, 2002] and should therefore be cogenetic. The substantial compositional zonation of some individual fallout tephras likely then reflects the compositional diversity of an individual magma batch prior to the eruption. The linear trends of major and trace elements versus MgO defined by the tephra glasses are typical for magma mixing rather than for fractional crystallization. Magma mixing is consistent with

Table 3. Standards Used for Boron and Lithium Calibration[a]

Standard	SiO_2 wt%	B ppm	$^{11}B^+/^{30}Si^{+e}$	Ion Yield[f]
JDF-D2[b]	50.8	1.11	0.000141	0.4581
UTR2[c]	74.4	14.3	0.001603	0.4910
NIST 612[d]	71.5	32.0	0.003738	0.4948
NIST 610[d]	72.0	351	0.037202	0.4950
Standard	**SiO_2 wt%**	**Li ppm**	**$^7Li^+/^{30}Si^{+e}$**	**Ion Yield[f]**
JDF-D2[b]	50.8	7.97	0.004331	1.065253
UTR2[c]	74.4	8.7	0.037832	1.707516

[a] Data were aquired during December 1997 to January 1998, and during September 1998 and October 1998.
[b] Basalt glass from the Juan de Fuca Ridge, developed by C. H. Langmuir. B and Li abundance data are WHOI in-house values.
[c] Montreal University standard, developed by J. Stix.
[d] NIST synthetic standard glasses, using WHOI in-house values.
[e] Measured ion ratios $^{11}B^+/^{30}Si^+$ and $^7Li^+/^{30}Si^+$.
[f] Secondary ion yield is B or Li normalized to Si, e.g., $[(B^+/Si^+)/(B/Si)]$.

Table 4. Repeatability of Laser Ablation ICP-MS Analyses on Standards and Samples, Including External Precision[a]

	BIR-g, n = 18			StHs6/80-G, n = 7			VE32, n = 8			69, n = 8	sk12n = 11		
	Ref. Value	This Study	s%	Ref. Value	This Study	s%	Ref. Value	This Study	s%	s%	s%	Percent in run precision	Percent repeatability
Cs	0.008	0.013	47.0	1.89	1.69	4.0		0.03	11.1	5.9	9.1	7.3	15.4
Rb	0.25	0.22	9.1	29.9	31.2	2.9	3.09	3.67	3.8	5.7	6.1	4.0	5.5
Ba	6.7	6.1	4.9	302	287	1.7	54.5	54.9	2.0	3.5	7.3	2.5	3.9
Th	0.033	0.030	12.6	2.22	2.32	4.0		0.40	7.3	7.5	14.3	4.0	9.1
U	0.009	0.023	21.1	1.03	0.97	7.6		0.15	6.0	5.9	24.0	5.9	12.9
Nb	0.54	0.51	5.2	7.1	6.4	3.4	6.55	6.06	2.0	2.8	3.9	2.5	3.4
Ta	0.042	0.037	9.8	0.418	0.428	6.1	0.41	0.40	3.5	11.3	7.7	7.0	7.7
La	0.59	0.59	4.8	11.9	12.1	1.2	6.3	6.6	1.3	3.2	6.0	2.4	3.3
Ce	1.9	1.8	5.6	25.7	25.0	1.4	16.89	17.42	2.3	2.9	8.1	2.4	4.1
Pb	2.9	3.8	8.5	10.2	10.7	5.3	0.72	0.89	6.6	4.7	16.9	3.3	8.4
Pr	0.37	0.36	6.0	3.17	3.03	1.1	2.67	2.68	2.4	3.3	6.8	2.7	3.9
Sr	110	106	2.1	486	469	0.9	169	177	0.4	3.4	5.1	2.3	2.4
Nd	2.37	2.35	4.3	12.7	12.7	1.7	13.72	14.31	2.1	2.6	6.9	2.3	3.5
Zr	15.5	13.6	2.3	120	115	3.9	129	121	3.3	3.8	3.9	2.1	3.5
Sm	1.12	1.08	5.9	2.79	2.71	4.7	4.27	4.45	1.8	4.7	6.4	2.7	4.7
Hf	0.58	0.56	5.7	3.16	3.07	2.5		3.32	3.0	4.6	8.5	3.6	4.9
Eu	0.53	0.50	5.3	0.97	0.93	2.9	1.5	1.6	3.0	3.4	6.8	3.1	4.3
Gd	1.88	1.82	5.6	2.64	2.57	2.5	5.71	5.76	2.4	3.1	8.3	3.2	4.4
Tb	0.36	0.34	4.3	0.372	0.362	3.8	0.97	0.98	1.6	3.5	7.5	3.1	4.2
Dy	2.51	2.64	3.9	2.19	2.28	3.9	6.16	6.82	2.0	2.1	7.6	1.9	3.9
Y	16.2	15.1	1.9	11.3	11.7	3.7	37.4	37.0	3.0	3.6	4.1	1.6	3.3
Ho	0.57	0.58	2.9	0.417	0.440	4.4	1.32	1.44	1.4	4.1	7.5	3.4	4.0
Er	1.66	1.72	4.7	1.17	1.21	4.4	3.69	4.08	2.0	3.1	9.0	2.5	4.6
Tm	0.255	0.256	4.0	0.167	0.179	2.5		0.60	1.9	4.0	6.6	3.4	3.8
Yb	1.65	1.75	4.5	1.11	1.18	3.5	3.56	4.03	2.4	4.6	7.4	3.4	4.5
Lu	0.253	0.263	5.3	0.168	0.174	3.4	0.54	0.60	3.8	3.4	7.0	2.7	4.6

[a] BIR-g is a fused glass of USGS BIR-1 rock standard used at Harvard. Reference values of StHs6/80-G are from *Jochum et al.* [2000]. VE32 is a natural mid-ocean ridge basalt glass developed by C. H. Langmuir. BIR-g and VE32 compositions are house values. Precision (s%) is reported as the percentage of one standard deviation of *n* repeat analyses of samples 69 and Sk12 that represent the extremes of the glass population investigated. Sample 69 is a vesicular, microlith-bearing rhyolite (Table 1), sample Sk12 is a homogenous, dense basalt glass from the Shikoku basin spreading center (DSDP site 442B). (Sk12 major elements in wt%: SiO_2 = 50.9; MgO = 6.27; trace elements in ppm: Cs = 0.057; Rb = 2.31; Ba = 17.0; Th = 0.22; U = 0.089; Nb = 2.24; Ta = 0.16; La = 4.32; Ce = 12.82; Pb = 0.76, Pr = 2.11; Sr = 156; Nd = 11.37; Zr = 102.3; Sm = 3.71; Hf = 2.70; Eu = 1.32; Gd = 4.82; Tb = 0.82; Dy = 5.88; Y = 33.0; Ho = 1.23; Er = 3.52; Tm = 0.53; Yb = 3.54; Lu = 0.53). Within run precision is based on repeat measurements during a run (a run comprises 20 analyses). Repeatability is the mean precision obtained from all run during the period of measurements (3 days).

the presence of strongly zoned plagioclase phenocrysts that show abrupt compositional changes (up to 30 mole% difference), inverse zonation and the melt inclusion-rich growth zones (''sieve-textures'') [e.g., *Straub and Layne*, 2002]). At present, as in any arc, the primary process of melt diversification in Izu VF magmas is much debated with no common consensus yet reached [e.g., *Schiano et al.*, 1995; *Prouteau et al.*, 1999; *Takagi et al.*, 1999; *Tamura and Tatsumi*, 2002]. However, basalt through rhyolitic tephras are also similar in their ratios of incompatible elements, quantities that should not be substantially affected by crystal fractionation, and therefore should reflect source variations.

[18] Quaternary lavas and the Neogene tephras are indistinguishable in incompatible trace element ratios, as well as in Sr, Nd, Pb and B isotopes [*Straub*, 1996; *Bryant et al.*, 1999; *Schmidt*, 2001; *Straub and Layne*, 2002] confirming the petrogenetic utility of these parameters. Figure 3 shows that the abundances of the incompatible trace elements of the glasses also define a much more limited and well defined range than the Quaternary Izu VF lavas. The glasses and lavas have the trace element pattern typical of arc lavas that is attributed to selective additions of Cs, Rb, Ba, Th, U, K, Pb, Sr, B and Li from the slab. The high B contents (10 to 40 ppm in the glasses; Figure 4), and the general covariance of B with the fluid-

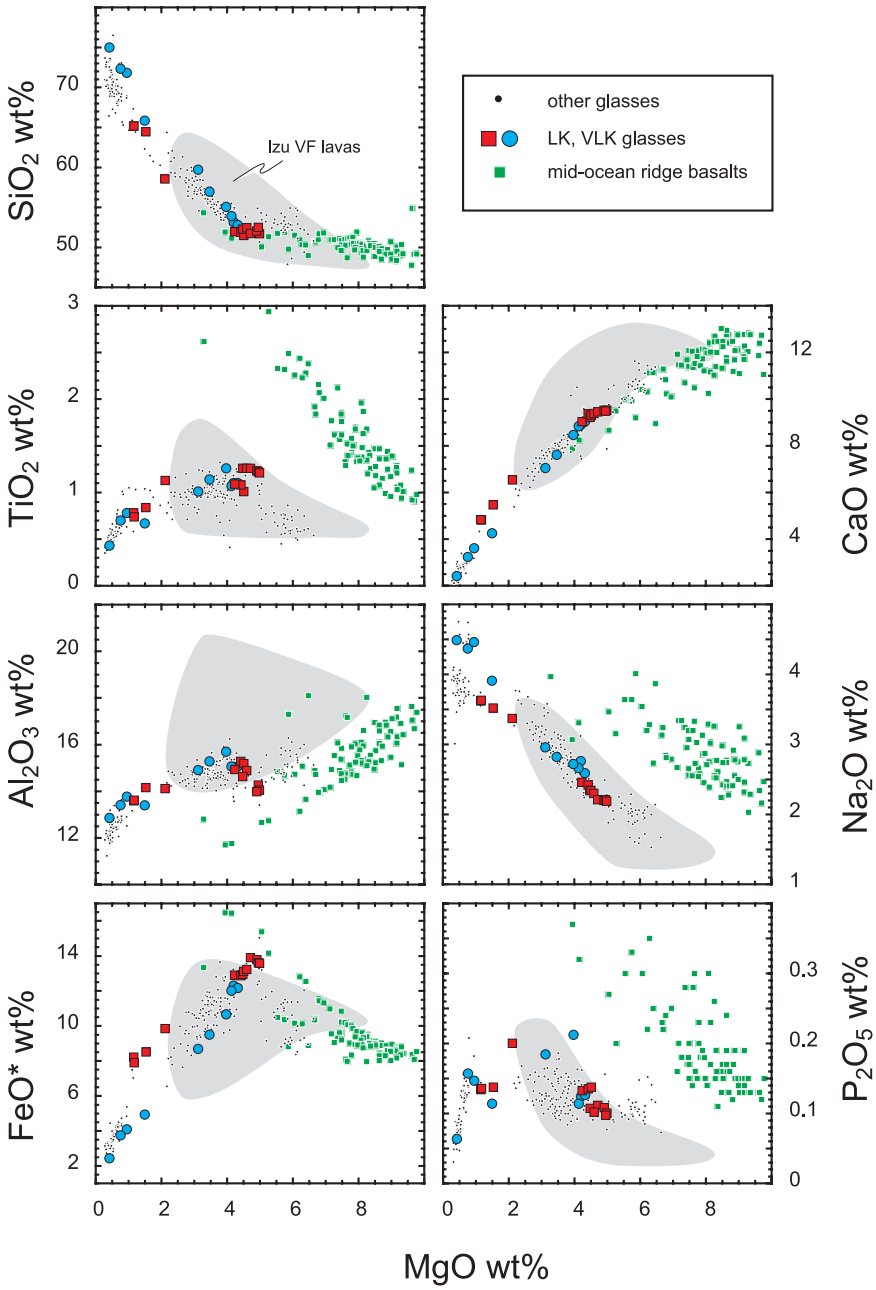

Figure 2. Major element compositions of 782A glasses (black filled circles) compared to Izu volcanic front lavas (gray shaded field) [*Taylor and Nesbitt*, 1998; *Langmuir et al.*, 2004] and MORB (small green squares) [*Niu and Batiza*, 1997]. VLK (blue circles) and LK (red squares) glasses analyzed by LA-ICPMS are singled out.

mobile large ion lithophile elements (= LILE) point unambiguously to the subducting slab as source of the LILE [*Straub and Layne*, 2002]. In contrast, the high field strength elements (HFSE) and the heavy rare earth elements (HREE) have abundances that are comparable to, or below, N-MORB. This is consistent with derivation of these elements from the mantle wedge [e.g., *Pearce and Peate*, 1995; *Elliott et al.*, 1997; *Hochstaedter et al.*, 2000].

3.2. Very Low-K (VLK) and Low-K (LK) Tephra Series

[19] Results from this study, and previous work [*Straub*, 2002], show that some tephra layers are homogenous, while others have a large range in

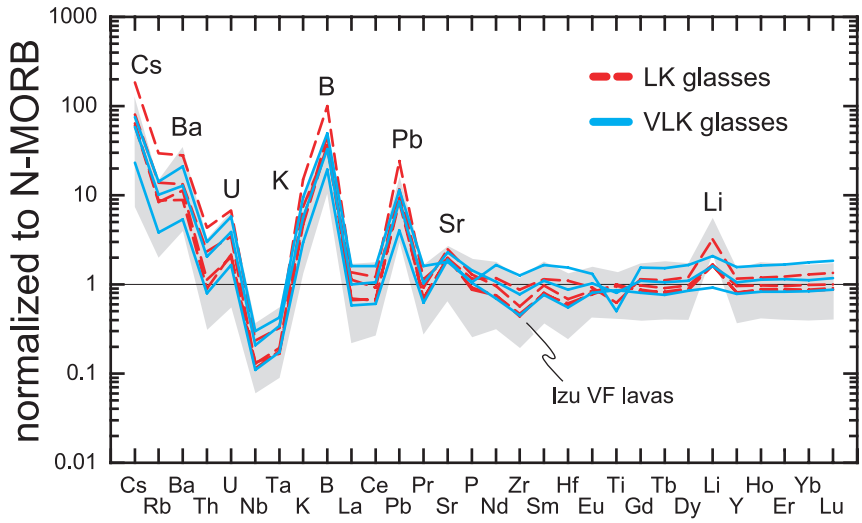

Figure 3. Incompatible trace elements abundances of 782A LK (red squares) and VLK (blue circles) glasses compared to Quaternary Izu VF lavas [*Taylor and Nesbitt*, 1998; *Langmuir et al.*, 2004]. The Ta data the Izu VF lavas are calculated using on the Nb of *Taylor and Nesbitt* [1998] and the average Ta/Nb of the Izu tephra glasses.

composition that is linear on variation diagrams. Two thirds of the individual layers examined have compositions that vary by 2 to 6 wt% in MgO, or up to 15 wt% in SiO_2 (Figure 5). In the K_2O versus MgO diagram, the glasses from layers with variable compositions form arrays of subparallel trends, that differ by a factor of ~2 in K_2O at a given MgO (Figure 5a), as do the Izu VF lavas. On the basis of K_2O, two representative trends can thus be defined that characterize this spectrum (Figure 5b): (1) a very low-K trend (VLK; blue) with K_2O increasing from 0.2 to 0.6 wt% between 5 and 2 wt% MgO; and (2) a low-K trend (LK; red) with K_2O increasing from 0.4 to 1.2 wt% over the same range of MgO. Other elements also vary with MgO. Figure 6 shows the elements in decreasing order of the magnitude of their variations. Cs, which varies by a factor of 2.4 is followed, in decreasing order, by Pb, Rb, B, K, Li, Ba, Th and finally La, which only varies by 20%. Sr does not differ systematically between the two glass series. Sr fractionation into plagioclase does not appear to cause this discrepancy, however, since basaltic andesitic VLK and LK glasses with no, or negligible, Eu anomalies have similar Sr contents. Unlike the fluid-mobile LILE, the REE, Hf, Zr, Nb, Ta and Y display similar abundances in LK and VLK glasses. Therefore the VLK and LK glasses differ systematically in their LILE/HFSE and LILE/REE ratios. The variable LILE/HFSE ratios are likely to reflect characteristics of the mantle source, since substantial fractionation of these elements is unlikely given the high degrees

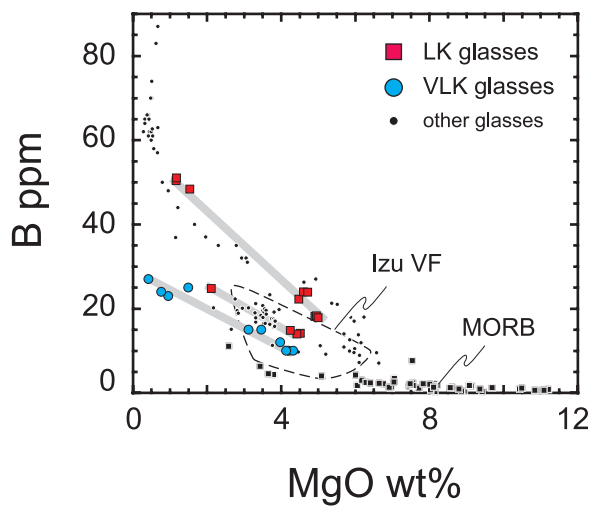

Figure 4. B ppm versus MgO wt% of Izu glasses and Izu VF compared to MORB (Izu VF and MORB data from *Ryan and Langmuir* [1993]). Grey lines highlight intralayer trends. High B contents and the general covariance with the LILE demonstrate the origin of these elements from slab. More details on B chemistry of the glasses are given in *Straub and Layne* [2002].

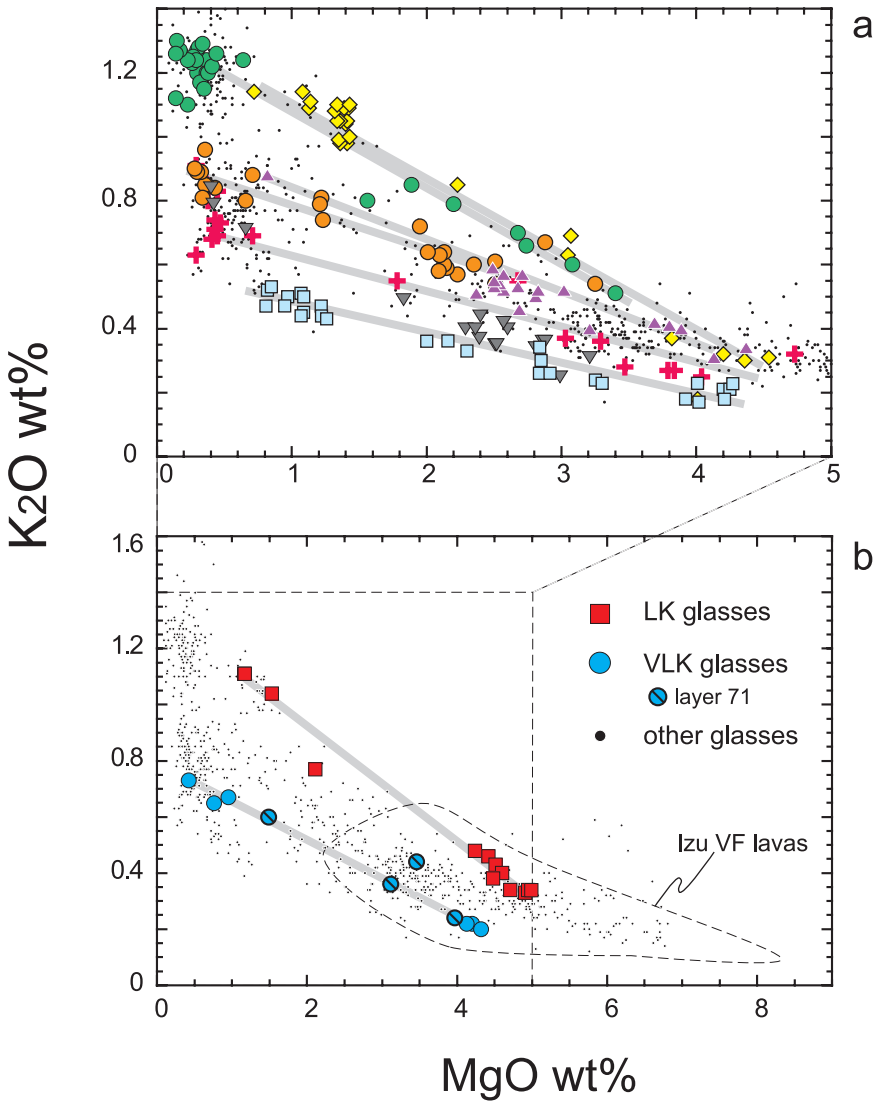

Figure 5. (a) The K_2O contents of the glasses in individual 782A fallout tephras show the compositional variation of individual magma batches prior to eruption. Small black dots indicate all Izu glasses. Large symbols underlain by grey lines highlight the trends within individual tephra layers. Data are from *Straub* [2003]. (b) Two representative trends were selected to characterize the spectrum of the Izu VF magmas: the low-K trend (= LK; red squares) and the very low-K trend (= VLK; blue circles). Grey lines highlight intralayer trends, and large symbols denote glass shards taken for SIMS and LA-ICPMS analyses. Slashed circles highlight an individual tephra fallout layer (sample 71). Glasses with >5 wt% MgO are mostly melt inclusions, which were not further considered in this study.

of melting (~20–25%) inferred beneath the Izu VF [*Plank and Langmuir*, 1988; *Hochstaedter et al.*, 2000].

4. Discussion

[20] The existence of the two magma series in a setting where fluid alone contributes to the chemical variations permits a determination of fluid composition that is much better constrained than other arc environments where multiple components often create complexities that are difficult to unravel.

4.1. Calculation Strategy

[21] The compositions of the individual slab components are calculated based on the concept that the subarc mantle source is a binary mixture of (1) an unmodified mantle wedge; i.e., mantle without

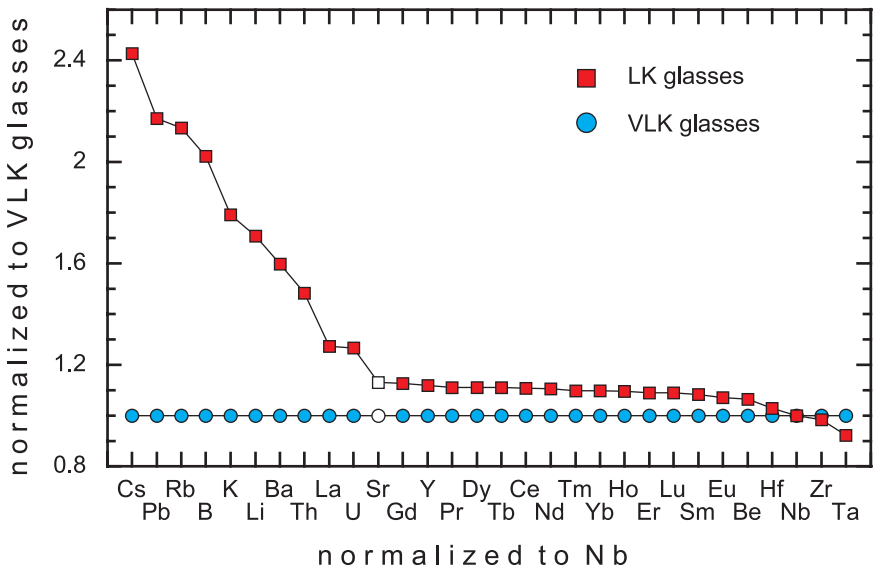

Figure 6. Differing abundances of incompatible elements of LK (red squares) and VLK (blue circles) glasses. Data are normalized to Nb in order to neutralize the effects of fractional crystallization. Open symbols indicate Sr that does not systematically differ between the two series as do the other elements.

any slab components ("background mantle") and, (2) the sum of individual components derived from the subducting slab ("total slab component"):

$$\text{subarc mantle(ARCs)} = \text{background mantle (BM)} + \text{total slab component (TSC)}$$

where:

$$\text{total slab component} = \text{metabasalt fluid (MBF)} + \text{metasediment fluid (MSF)} + \text{sediment melt (SM)}$$

Thus the abundance of an element in the arc source is (see Table 5 for abbreviations):

$$c_{ARCs} = c_{BM} * x + c_{TSC} * y \quad (1)$$

where $x + y = 1$, or:

$$c_{ARCs} = c_{BM} * x + (c_{SF} * a + c_{MBF} * b + c_{SM} * c) * y \quad (2)$$

where $x + y = 1$ and $a + b + c = 1$.

[22] If one slab component is missing (i.e., the sediment melt at the Izu VF), then c is zero. The strategy in this paper is to calculate first the composition of the total slab component, and then partition it into the individual fluid and melt components. In order to obtain the total slab component, the following variables must be known: (1) composition of the arc source mantle, (2) composition of the background mantle, and (3) the mixing ratio of the total slab component and background mantle. All of these can be constrained for the Izu VF, as defined below and at greater length in appendix A. The composition of the arc source mantle can be determined by simple inversion of the tephra compositions using the batch melting equation and known partition coefficients. The uniform concentrations of the elements that are not fluid mobile suggests the extent of melting

Table 5. Abbreviations Used in Equations

	Concentration of an Element in
c_{ARCs}	arc source mantle = subarc mantle including all additions from slab
c_{BM}	background mantle = arc mantle source without additions from slab
c_{TSC}	total slab component = entirety of components added from slab
c_{SF}	sediment fluid = fluid released from the subducting sediment
c_{MBF}	metabasalt fluid = fluid released from the metabasalt
c_{SM}	sediment melt = melt from the subducting sediment

Table 6. Trace Element Compositions of Slab and Wedge End-Members for the Neogene Izu VF[a]

	1 Izu Trench Sed[b]	2 Meta-Sed Fluid[c]	3 Avg Mesoz Crust[d]	4 Meta-Basalt Fluid[e]	5 Avg Izu VF[f]	6 Avg Izu VF Source[g]	7 Izu Background Magma[h]	8 Izu Background Mantle[i]	9 Bulk Partition Coeff.[j]	10 Avg Comp. Fluid[k]	11 Perc% Added From slab[l]
Cs	3.65		0.149		0.32	0.0639	0.0007	0.0001	0.00037*	3.9±1.6	99.7±0.1
Rb	52.51		9.9		3.50	0.70	0.057	0.011	0.00037	42±17	98.1±0.9
Ba	830		13.0		45.4	9.10	0.646	0.129	0.00037	544±153	98.5±0.5
Th	5.67		0.17		0.11	0.023	0.012	0.0025	0.00049	1.3±0.5	88.4±3.4
U	1.53		0.13		0.09	0.017	0.0048	0.001	0.00082	1.0±0.2	94.2±1.2
Nb	6.53		3.6		0.24	0.048	0.239	0.048	0.0011	0	0
Ta	0.472		0.20		0.020	0.004	0.020	0.0041	0.0011*	0	0
K	13414		3429		2164	439	160	32.5	0.00378*	24657±9027[+]	91.9±2.8
La	37.98		3.93		1.43	0.29	0.950	0.195	0.00646	5.9±3.2	31.8±10.6
Ce	47.26		12.43		4.11	0.89	3.53	0.746	0.01429	4.1±4.1	13.8±6.5
Pb	16.67		0.46		1.80	0.40	0.16	0.036	0.03037	22.3±8.7	90.0±4.1
Sr	158		112		153	33	47.7	10.4	0.02145	1384±233	68.5±3.3
Nd	44.5		12.3		4.49	1.00	4.3	0.96	0.03037	2.5±2.6	4.0±4.1
Sm	9.7		4.5		1.72	0.41	1.8	0.43	0.04486	<0	–
$^{87}Sr/^{86}Sr$	0.70958	0.70958	0.7028	0.7032	0.7035	0.7035	0.7028	0.7028		0.7039	
$^{143}Nd/^{144}Nd$	0.51233	n.a.	0.51319	n.a.	0.51308	0.51308	n.a.	n.a.		n.a.	
$^{206}Pb/^{204}Pb$	18.61	18.61	18.45	18.1	18.39	18.39	18.3	18.3		18.42	
$^{207}Pb/^{204}Pb$	15.61	15.61	15.45	15.44	15.51	15.51	15.5	15.5		15.55	
$^{208}Pb/^{204}Pb$	38.64	38.64	37.64	37.6	38.21	38.21	38.0	38.0		38.31	
Pb and Sr abundances of fluids											
Sr		~2960		~1300	–	–	–	–	–	~1383	–
Pb		280		8.7	–	–	–	–	–	~22.3	–

[a] All element values in ppm. n.a. not available.
[b] Column 1, Izu trench sediment after Plank and Kelley (manuscript in preparation, 2003) and *Hauff et al.* [2003].
[c] Column 2, metasediment fluid (see Table 7 for composition).
[d] Column 3, average composition of NW Pacific Mesozoic ocean floor basalts.
[e] Column 4, metabasalt fluid (see Table 7 for composition).
[f] Column 5, average of primitive magmas from the Izu VF, based on fractionation-corrected composition of basaltic andesitic glasses.
[g] Column 6, Izu VF mantle source, reconstructed from average Izu VF (column 5), assuming 20% degree of partial melting (batch melting), a depleted peridotite (OLIV:OPX:CPX = 60:25:15) and the bulk partition coefficients of column 9.
[h] Column 7, Izu "wedge magma," i.e., magma from unmetasomatized background mantle wedge. See appendix for determining isotopic compositions.
[i] Column 8, background mantle wedge, reconstructed from Izu wedge magma (column 7), as in footnote 6.
[j] Column 9, bulk partition coefficients (D's) from *Donnelly* [2002]. Asterisk indicates $Kd_{Cs} = Kd_{Rb}$, $Kd_{Ta} = Kd_{Nb}$, Kd_K interpolated between Kd_{Nb} and Kd_{La}.
[k] Column 10, average of composite fluid (5% metasediment fluid, 95% metabasalt fluid), calculated using 1.6% of slab fluid in wedge (98.4%). Crosses indicate $K_2O = 3.0 \pm 1.1$ wt%.
[l] Column 11, percentage of slab-derived elements in Izu VF magmas.

for both LK and VLK series is the same. The background mantle is constrained by the very low Nb and Ta to be highly depleted MORB, and the systematics of MORB compositions permit estimates of all other elements. Mixing ratios are constrained from the isotopic compositions of the tephra samples [*Schmidt*, 2001]) as well as the subducted sediment in this region [*Hauff et al.*, 2003; Plank and Kelley, manuscript in preparation, 2003] and various analyses appropriate to constrain the wedge background composition [e.g., *Hochstaedter et al.*, 2000; *Ishizuka et al.*, 2003]).

4.2. Characterization of the Slab Fluids at the Izu VF

4.2.1. Mixing Calculations

[23] Several previous studies have used Pb isotope systematics to identify the total slab component at the Izu VF as a mixture of two slab fluids, essentially a "composite fluid," consisting of metabasalt fluid and metasediment fluid components. These studies also presented compositions of the Izu VF background mantle and the Izu VF mantle source, as well as the mixing ratios of the two slab fluids, the background mantle and the

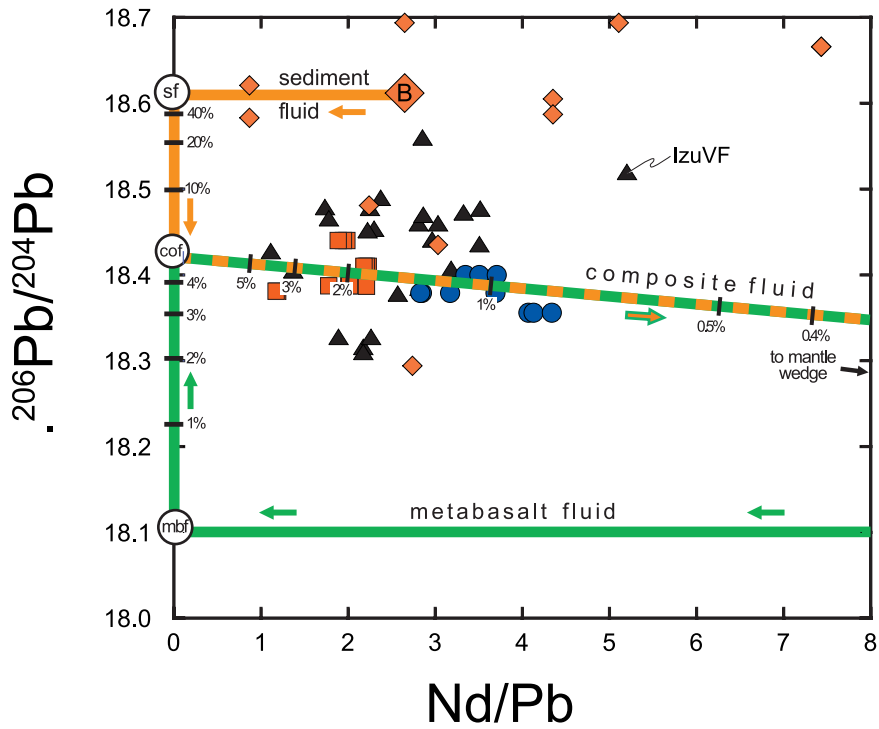

Figure 7. Nd/Pb versus $^{206}Pb/^{204}Pb$ isotope ratios. The LK (red squares) and VLK (blue circles) glasses are homogenous in Pb isotopes and Nd, but Pb abundances differ by a factor of ~2 (Figure 6). sf, metasediment fluid (orange); mbf, metabasalt fluid (green); cof, composite fluid (orange-green). Brown diamonds trench sediment. B bulk trench sediment. Black triangles Izu VF volcanics. The intersection of the VLK and LK glass array with the y axis defines the Pb isotope ratio of the composite fluid ($^{206}Pb/^{204}Pb$ ~18.42; Nd/Pb ~0). Corresponding diagrams can be drafted for $^{207}Pb/^{204}Pb$ ~15.55 and $^{208}Pb/^{204}Pb$ ~38.31. Tick marks on y axis indicate the proportion of metasediment fluid in composite fluid. Tick marks on horizontal line indicate the proportion of composite fluid in the background mantle. See appendix for data sources and for details of modeling.

composite fluid [e.g., *Taylor and Nesbitt*, 1998; *Hochstaedter et al.*, 2000, 2001; *Schmidt*, 2001; *Ishizuka et al.*, 2003]. However, because each of these studies used different approaches and mixing end-members, and consequently arrived at different end-member compositions and mixing proportions, we repeated the modeling to obtain an internally consistent model prior to characterizing the Izu VF slab fluids in detail. The modeling procedures are summarized in appendix A, and the results are presented in Table 6. In short, the composite fluid was found to be a mixture of 95% metabasalt fluid and 5% metasediment fluid (Figures 7 and A1). The percentage of composite fluid in the Izu source that is able to account for the isotopic variations of the tephra samples ranges from 0.8% to 3.7%, with an average of 1.6% (Figure 7).

4.2.2. Variable Amounts of Fluid in Source

[24] While the Quaternary Izu VF lavas obviously reflect the isotopically diverse subarc mantle and slab components [*Taylor and Nesbitt*, 1998; *Ishizuka et al.*, 2003], the tephra record is much more consistent in trace elements and isotopes [*Straub*, 1996; *Bryant et al.*, 1999]. The uniformity of the tephra is clearly evident in the

Figure 8. LILE versus LILE diagrams of Izu background mantle (W, wedge), and mantle source abundances of basaltic andesitic VLK and LK glasses only. Prior to calculating the source abundances, the glass compositions were corrected for fractionation as described in appendix A2.1. The glasses plot on a mixing line between the wedge and the slab component (= composite fluid) (outside diagrams, black arrow). Tickmarks indicate the proportion of composite slab component in source. Thick cross denotes average percentage (1.6%) of composite fluid (cof) in source. Gray shaded range show the range of LILE/LILE of the composite fluid. See text for discussion.

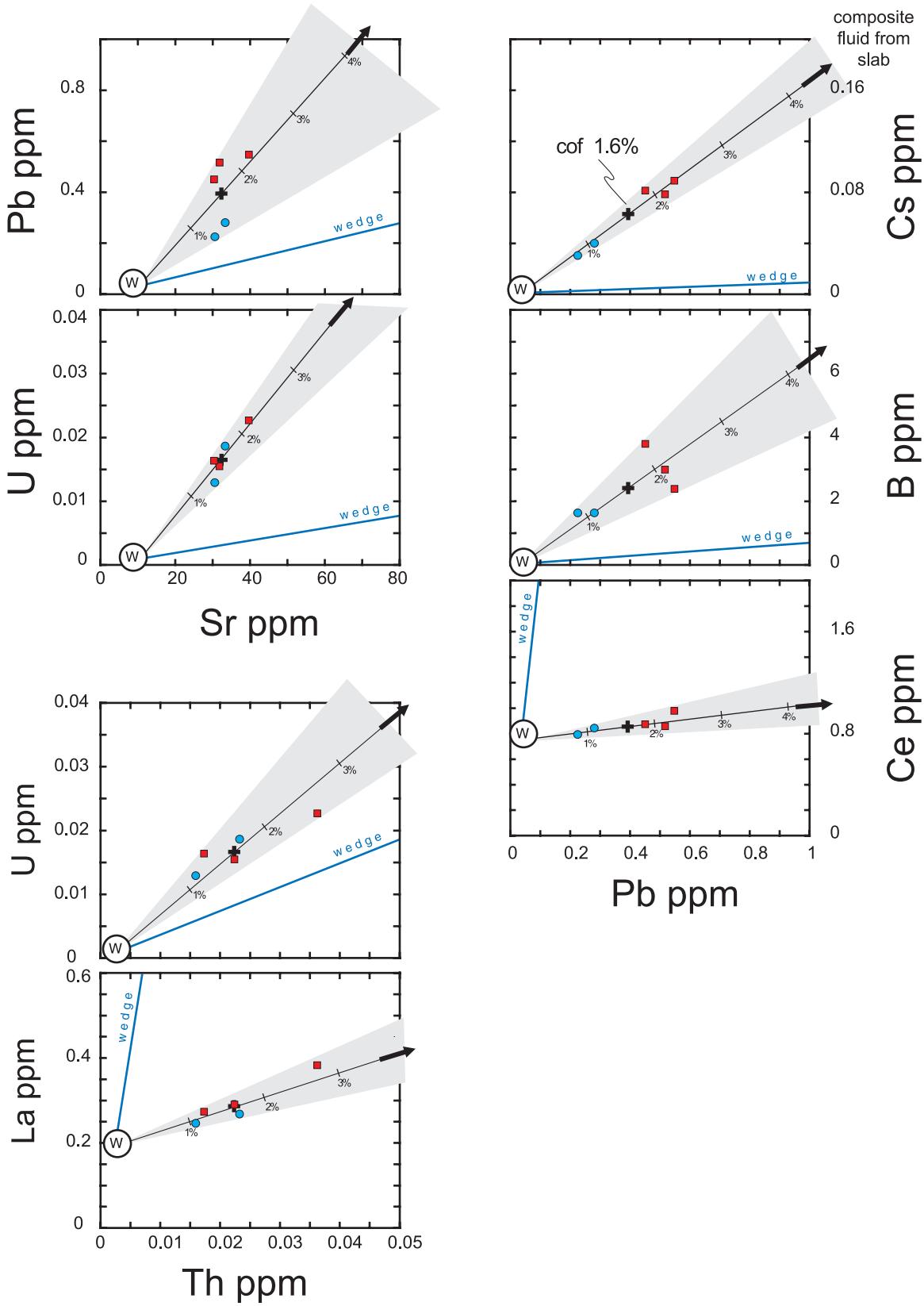
Pb ppm
U ppm
Sr ppm
U ppm
La ppm
Th ppm
Cs ppm
B ppm
Ce ppm
Pb ppm
composite fluid from slab
cof 1.6%
wedge
W
1%
2%
3%
4%

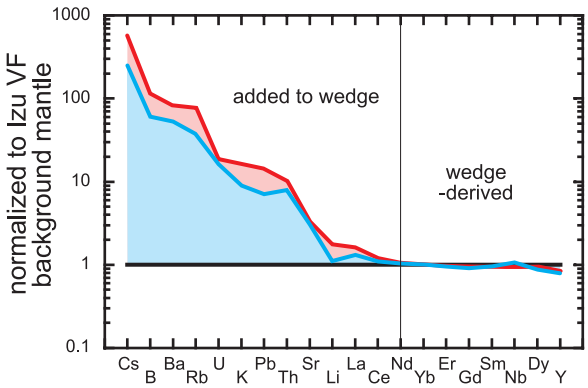

Figure 9. Slab contributions of recycled elements relative to the Izu VF background mantle. Average of VLK (blue) and LK (red) basaltic andesitic glasses are used to calculate two representative composite fluids in order to demonstrate effect of fluid variations.

Nd/Pb versus Pb isotope diagram, where the tephra glasses cut through the field of the isotopically more variable Izu VF lava samples in a similar Nd/Pb range (Figures A2 and 7). An important aspect is that the Nd/Pb of the VLK glasses is consistently lower than the LK glasses at similar Pb isotope ratios. Since the VLK and LK series have similar Nd abundances (Figure 6), the horizontal dispersion in Nd/Pb is caused by variations in the Pb abundance, which are controlled by the slab flux. Consequently, the variable Nd/Pb must reflect a different amount of composite fluid in the source, varying by a factor of 2 between the VLK (~1.1% composite fluid in source on average) and LK series (~2.2%) (Figure 7; see appendix for mixing calculations).

[25] Mixing variable amounts of fluid should also lead to linear mixing arrays on element-element plots for those elements carried in the fluid. Indeed, the source abundances, calculated from the fractionation-corrected basaltic andesitic VLK and LK glasses, plot on linear arrays between the depleted background mantle wedge (W) and the LILE-rich composite fluid from slab (thick arrow in Figure 8). The LK glasses are relatively more enriched in the fluid component. Although there is some variability in these diagrams, any LILE/LILE of the Izu VF composite fluid (1) is well within the range of the Quaternary Izu VF magmas, (2) has a narrow range compared to global arc magmas, and (3) clearly differs from the mantle wedge. Thus the composite slab fluid displays a relatively limited range, and hence a surprising overall uniformity in trace elements.

[26] On the basis of the proportions constrained by isotopes and the linear arrays shown in Figure 8, the average composition of the composite fluid can be calculated, as given in column 10 of Table 6. The percentages of the recycled elements contributed from the slab are shown in column 11 of Table 6. In Figure 9, the composite fluid composition is shown, normalized to Izu VF background mantle. Despite the small fraction of composite fluid in the mantle source (average 1.6%), Figure 9 demonstrates clearly that the composite fluid dominates the Izu VF budget of Cs (~99% derived from slab), B (~99%), Ba (~98%), Rb (~98%), U (~94%), K (~91%), Pb (~90%), Th (~88%) and Sr (~69%). The slab contributions to Li (~37%) and the light REE La (~32%), Ce (~14%) and Nd (~4%) are moderate. No slab contributions are apparent for Nb and Ta (by definition), or for the other middle and heavy REE, consistent with these elements being entirely wedge-derived (Figure 10).

[27] This composition of the composite fluid is supported by comparison to forward calculated

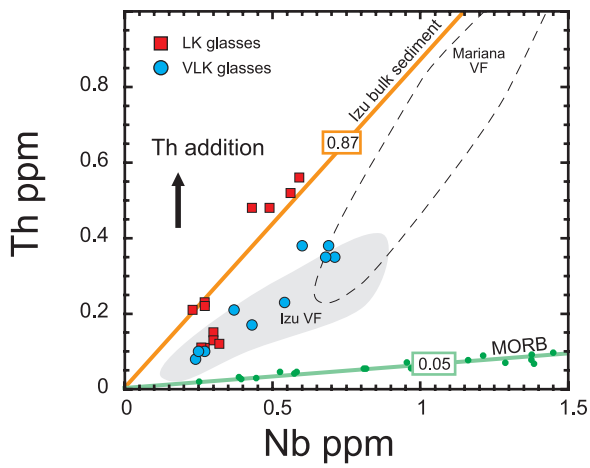

Figure 10. The Th versus Nb diagram show that the Nb abundances of the Izu glasses are similar low or lower than the most depleted MORB. Therefore it is unlikely to the extreme that any Nb was added from slab, in contrast to Th that is higher than MORB at a given Nb. Numbers in rectangles indicate Th/Nb ratios of bulk trench sediment and MORB. Izu VF data are from *Taylor and Nesbitt* [1998] and *Langmuir et al.* [2004], Mariana VF are from *Elliott et al.* [1997].

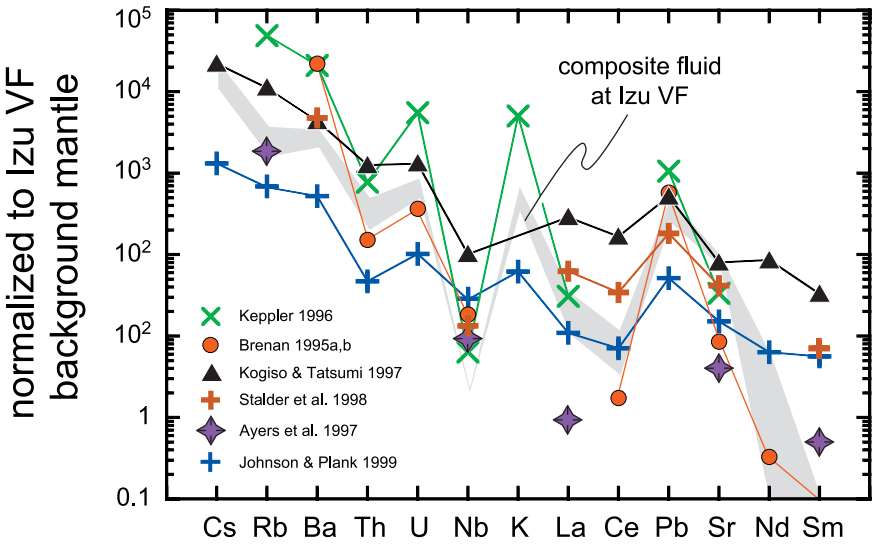

Figure 11. Average composite fluid (gray shaded range; ±one standard deviation) compared to forward calculated fluids using experimental fluid/solid partitioning experiments and assuming 0.5% fluid release. A mixture of 6% trench sediment (Table 6, column 1) and 94% metabasalt (Table 6, column 3) was taken as original solid. All data are normalized to Izu background mantle (column 8, Table 6). *Brenan et al.* [1995a, 1995b]: D's calculated using a source composition of 59% garnet, 39% pyroxene, 2% rutile. *Stalder et al.* [1998]: D's calculated using a source composition of 59% garnet, 39% pyroxene, 2% rutile. *Ayers et al.* [1997]: average D from nine fluid/peridotite partitioning experiments. *Johnson and Plank* [1999]: average D's from the two-fluid/sediment partitioning experiments. *Keppler* [1996]: average D's of partitioning experiment containing 5m (Na,K)Cl fluid. *Kogiso et al.* [1997]: D's calculated assuming 5% fluid loss from capsule.

compositions based on the fluid/solid partition coefficients from various experimental studies, and using an average bulk slab composition as source (Figure 11) [*Johnson and Plank*, 1999; *Ayers et al.*, 1997; *Kogiso et al.*, 1997; *Brenan et al.*, 1995a, 1995b; *Stalder et al.*, 1998]. Despite the considerable range in the magnitude of the bulk partition coefficients (Ds), owing to the widely differing experimental techniques and starting materials, the experimental fluids reproduce key features of the composite fluid remarkably well. These are: (1) the enrichments in Cs, Rb, Ba, U, K, Pb, Sr relative to Th, Nb, and the LREE, (2) the low U/Th ratios, and (3) the high Pb/Sr ratios. In addition, all experimental fluids show the elevated LILE/Th and LILE/LREE ratios, since lesser amounts of Th, U and LREE are mobilized. Only the depletion of Rb relative to Ba and Cs in the composite fluid is not well reproduced in the experiments. Since this depletion is a signature of the Izu trench sediment, perhaps it was inherited from the metasediment component fluid, rather than being created by the processes of dehydration.

[28] Normalizing the VLK and LK glasses to each other shows the relative fluid mobilities for the different elements, given the argument that only different amounts of a single fluid component create the differences between the two magma series. This inferred sequence of fluid-mobility is apparent in Figure 6; showing Cs as the most fluid-mobile element, followed by Pb, Rb, B, K, Li, Ba, Th, La and U. However, no information on the relative fluid mobility of Sr can be derived on this basis, since Sr does not differ systematically in the VLK and LK series.

[29] The data and modeling then suggest a very coherent behavior of elements in their overall mobility in the fluid phase that is largely consistent with previous studies and experimental data. Some elements, such as Cs, B and Pb are highly concentrated in the fluid phase, others such as U are modestly concentrated. In contrast to some previous conclusions, however [e.g., *Elliott et al.*, 1997] the Izu data suggest that even Th can be slightly mobile in the fluids, although the fluids certainly have high Cs/Th and U/Th ratios.

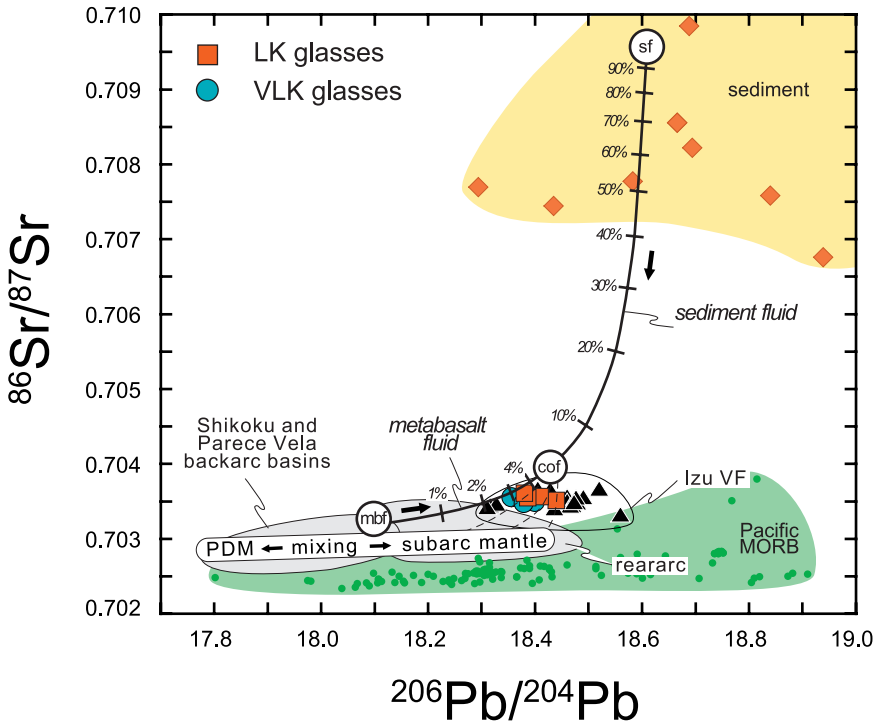

Figure 12. $^{87}Sr/^{86}Sr$ versus $^{206}Pb/^{204}Pb$-isotope diagram. The mixing curve is constructed for Sr = 1300 ppm in the metabasalt fluid, and Sr = 2960 ppm in the metasediment fluid. Tick marks indicate percentage of metasediment fluid in composite fluid. The average Sr isotope ratios of n = 8 of Izu rear-arc magmas with Nd/Pb > 16 was taken for the subarc mantle component ($^{87}Sr/^{86}Sr$ = 0.7028). The stippled mixing lines are optimized to pass through the tephra glasses that represent the average Izu VF compositions. Mixing trends through the entire Izu VF field require some larger, but still feasible variations in the isotopic and trace element compositions of the mixing end-members. See appendix and Table 6 for data sources and details of modeling.

4.2.3. Distinguishing Metabasalt and Metasediment Fluid Components

[30] The fluid composition determined above is the composite fluid derived by mixing of fluids evolved from both metasediment and metabasalt. The metasediment and metabasalt have very different Pb isotope ratios (Figures 7, A1, and A2), implying that a change in their relative proportions would cause substantial Pb isotope (and concentration) variations in composite fluid compositions. Instead, the tephra data indicate a highly uniform composite fluid compositions, which argues that the slab source components and the fluid mixing ratios have been uniform for 15 million years. Owing to its much larger volume, the metabasalt fluid (~95% of composite fluid) contributes a larger amount (~37%) of the Pb to the Izu VF although it's Pb abundance is only ~3% of the metasediment fluid Pb. Given the strong correlations of Pb and the other LILE (excepting Sr), it appears likely that the metabasalt fluid also carries significant amounts of the other fluid-mobile LILE. In the following we use the excellent correlations between Pb and other elements to estimate the full range of the LILE in the two slab fluids.

4.2.3.1. Origin of Sr

[31] Although Sr concentrations do not covary simply with Pb isotopes, the slab sources of Sr can be identified using the Sr isotope data. We infer the approximate Sr content of the two fluids by inverse methods. Knowing the Pb and Sr isotope ratios, the Pb contents, and the mixing ratio of the two fluids, their Sr contents can be estimated by fitting mixing curves in the Pb-Sr isotope diagram (Figure 12). The metasediment-metabasalt mixing curve in Figure 12 is fitted to pass just above the field of the Izu VF magmas, assuming that the $^{87}Sr/^{86}Sr$ ratio of the metabasalt fluid from altered Pacific MORB is approximately ~0.7032 [*Janney*

and Castillo, 1997; *Hauff et al.*, 2003]. Because it makes up such a large proportion of the total fluid and Sr concentrations in basalt and sediment do not differ greatly, the metabasalt fluid must have Sr contents similar to the composite fluid. Feasible mixing curves are obtained for a metabasalt fluid of Sr ~1440–1460 ppm, and a metasediment fluid of Sr ~1000–3000 ppm. Clearly, the metabasalt Sr dominates the composite fluid (providing 90–96% of the Sr), whereas the Sr contribution from the metasediment fluid is small. Even if the unradiogenic Sr from the wedge ($^{87}Sr/^{86}Sr$ ~0.7029; ~32–33% of total Sr at the Izu VF) is taken into account, it shows that the metabasalt is still the major source of the Sr in the Izu VF magmas (~61–64% of total Sr).

[32] It is noteworthy that these Sr calculations cannot be verified using the available experimental data on Sr partitioning into fluid. The available solid/fluid partition coefficients for Sr [*Brenan et al.*, 1995a, 1995b; *Johnson and Plank*, 1999; *Stalder et al.*, 1998] mostly yield Sr abundances for the metasediment and metabasalt fluids too low to account for the high Sr of the composite fluid (~1450 ppm). This is not a problem restricted to our data set, however, since the available partition coefficients are not consistent with the overall high Sr/Nd ratios observed in arc volcanics.

4.2.3.2. Origin of the Other LILE

[33] The procedure to determine the abundances of the other LILE (= Cs, Rb, Ba, U, Th, K, LREE) in the two slab fluids is to (1) forward calculate the metasediment fluid, and then (2) to calculate the metabasalt fluid by mass balance from the composite fluid. Unfortunately, the only existing set of experimental solid/fluid partition coefficients (D's) for sediment dehydration by *Johnson and Plank* [1999] is not without problems. These partition coefficients were obtained from two runs at temperatures of 650°C and 700°C, respectively, on splits of a single sample of pelagic clay, but show differences in the D's s that cannot be attributed to the temperature difference only. Moreover, the *Johnson and Plank* [1999] D's are mostly much higher than the D's calculated based on solid/fluid experiments of silicate minerals (Figure 11). This

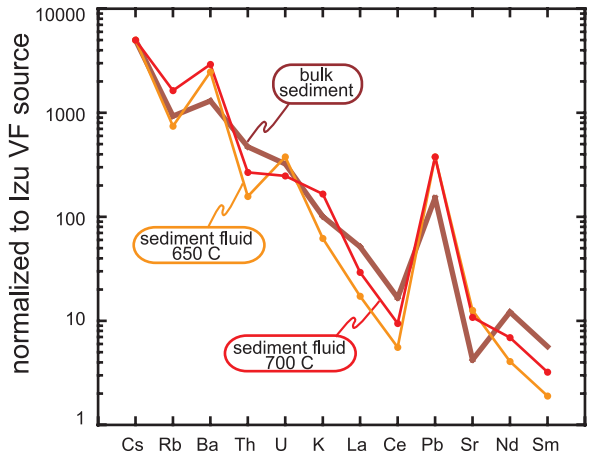

Figure 13. Fractionated fluids of Izu bulk subducting sediment calculated with the preferred bulk solid/fluid partition coefficient of *Johnson and Plank* [1999] for the solid/fluid partitioning experiments carried out at 650°C and 700°C. Data are scaled to Cs as one of the most fluid-mobile elements in order to highlight fractionation effects.

may be a consequence of incomplete fluid extraction from the clay residue into the diamond trap. In fact, the $D^{Pb}_{sed/fl}$'s of *Johnson and Plank* [1999] are too high to account for the high Pb of the metasediment fluid required by mass balance (see appendix A1.2). However, the sense of the Pb/LILE fractionation is similar the two runs (Figure 13), suggesting that the *Johnson and Plank* [1999] experiments record at least qualitatively the Pb/LILE fractionation during dehydration.

[34] To try to make use both of the Johnson and Plank experiments and other data, we took the ratio of the $D^{Pb}_{ec\ log/fl}$ = 0.05 calculated after *Brenan et al.* [1995a], to the two $D^{Pb}_{sed/fl}$'s of *Johnson and Plank* [1999] ($D^{Pb}_{sed/fl}$ = 0.64 at 650°C, and $D^{Pb}_{sed/fl}$ = 0.94 at 700°C) and applied this same factor to the other elements. The factors were 10.8 (650°) and 15.6 (700°), respectively. In order to determine how much our results depend on these uncertainties, we forward calculated three different metasediment fluids (Figure 14) for an arbitrarily chosen fluid fraction of 1% (F = 0.01) from the bulk trench sediment. In the first calculation, we assumed that the Pb/LILE of sediment are not fractionated during dehydration (i.e., the Pb/LILE ratios of the fluids remain the same as in the metasediment). In the second and third calculation we included the

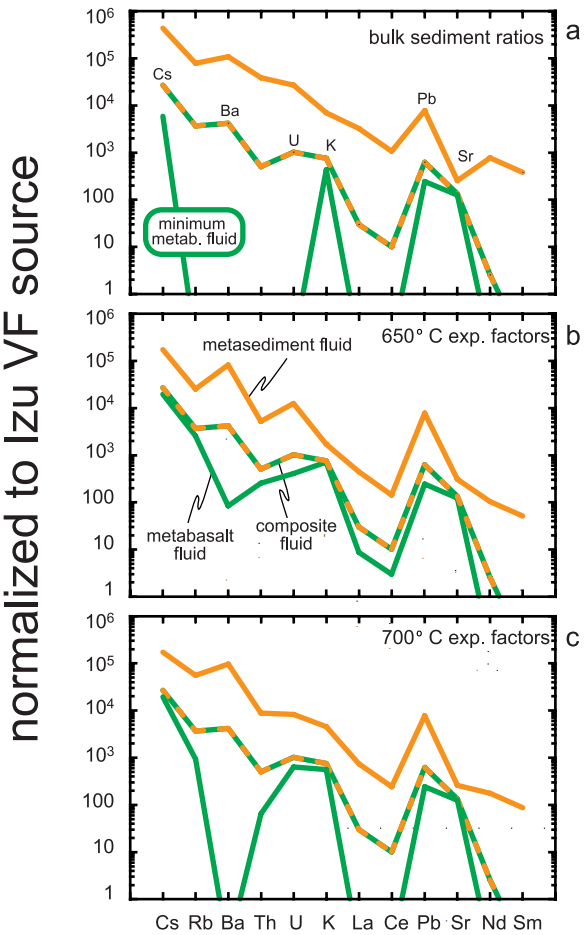

Figure 14. Fractionation patterns of the composite slab fluid compared to the patterns of metasediment fluid and of metabasalt fluid. Figure 14 (a) "Minimum metabasalt fluid," based on $D^{Pb}_{eclog/fl} = 0.05$ after *Brenan et al.* [1995a], and assuming no Pb/LILE fractionation during sediment dehydration. Metabasalt fluid calculations in Figures 14 (b) and (c) are based on the same $D^{Rb}_{eclog/fl} = 0.05$, but take into account the Pb/LILE fractionation measured by *Johnson and Plank* [1999] at 650°C (Figure 14b) and 700°C (Figure 14c).

Pb/LILE fractionation factors from the 650°C and 700°C experiments of *Johnson and Plank* [1999], respectively.

[35] The results of the partitioning calculation are shown in Figures 14a–14c. In Figure 14a (unfractionated Pb/LILE), the contribution of the metasediment fluid is highest, and the contribution of the metabasalt fluid is lowest. This "minimum" metabasalt fluid carries only Cs, K, Pb and Sr (Figure 14a; Table 7). The other two calculations yield mostly similar or higher abundances of these elements in the metabasalt fluid and show transport of Ba, Th, U and the LREE as well (Figures 14b and 14c; Table 7). In all three cases, the metasediment fluid is enriched by about an order of magnitude relative to the metabasalt fluids, excepting Sr that is only ~2 times higher in the metasediment fluid. Because of its large volume, however, the metabasalt fluid contributes large amounts of LILE to the composite fluid [e.g., Cs (21–68%), Rb (25–66%), Ba (0–2%), U (38–60%), K (70–89%), Pb (~37%) and Sr (~88–90%) (Table 7)]. Further, the K and Sr of the metabasalt fluid must be the cause for the positive K and Sr anomalies in the composite fluid, because the metasediment fluids have no K anomaly, and have a negative Sr anomaly. The Sr provenance from metabasalt is expected from experimental work [e.g., *Brenan et al.*, 1995a; *Kogiso et al.*, 1997], and from the observed Sr isotope chemistry of arc magmas. However, identifying metabasalt as the dominant K source is new, since no experimental data on solid/fluid K partitioning exists. In fact, as in the case of Sr, the abundances of K in the metabasalt fluid are so high, that after correction for the wedge contribution, most of the K (64–82%) at the Izu VF originates from the metabasalt (Table 7).

[36] Figures 14b and 14c indicate that some transport of Th and LREE in the metabasalt fluid. However, this result must be treated with caution, owing to the uncertainties of the D's, and the low contents of Th, U and the LREE in the fluids. In glasses with $SiO_2 < 60$ wt% (that are not saturated with apatite), the La/Nd correlates inversely with the Ce anomaly (= Ce/Ce*). This points to the metasediment as source of the LREE (Figure 15), as well as for Th as indicated by the (weak) correlation of Th/Nd versus Ce*.

4.2.4. "Arc Signature" of the Metabasalt Fluid

[37] Similar to the composite fluid, all metabasalt fluids have high ratios of Cs, K, Pb and Sr to Th and U, and, in two cases, elevated U/Th. The only significant difference is the low, or missing, Ba of the metabasalt fluid. Because of the calculation procedure, the low Ba of the metabasalt fluids is a direct consequence of the high Ba of the Izu trench

Table 7. Elemental Compositions of Metabasalt and Metasediment Fluids Calculated for the Three Different Sets of Pb/LILE Fractionation Data[a]

	1	2a	2b	2c	2d	3a	3b	3c	3d	4a	4b	4c	4d
	Avg Comp. Fluid Cof[b]	Meta-Sed Fluid (max)[c]	Meta-Basalt Fluid (min)[d]	Perc% mbf to Cof[e]	Perc% mbf to Izu VF[f]	Meta-Sed Fluid[g]	Meta Basalt Fluid[h]	Perc mbf to Cof[i]	Perc mbf to Izu VF[j]	Meta-Sed Fluid[k]	Meta Basalt Fluid[l]	Perc mbf to Cof[m]	Perc Mbf to Izu VF[n]
Cs	3.9	61	0.84	21	21	25	2.8	68	68	25	2.8	68	68
Rb	42	882				285	29	66	65	630	11	25	24
Ba	544	13947				10665	11	2	2	12618			
Th	1.3	95				13	0.6	48	43	22	0.2	12	11
U	1.0	26				12	0.4	38	36	8	0.6	60	56
Nb	0												
Ta	0												
K	24657	225351	14094	54	50	55914	23012	89	82	149714	18075	69.6	64
La	5.9	638				86	1.7	27	9	146			
Ce	4.1	794				107	2.2	28	4	182			
Pb	22.3	280	8.7	37	34	280	8.7	37	34	280	8.7	37	34
Sr	1384	2648	1317	90	62	3187	1289	88	61	2734	1313	90	62
Nd	2.5	747				101				171			
Sm	<0	163				22				37			

[a] All element values in ppm. For all calculations: Mixing ratio metabasalt fluid: sediment fluid = 0.05: 0.95. Mixing ratio Izu background wedge: composite fluid = 0.984: 0.016.
[b] Column 1, average composite fluid (cof) from column 10 in Table 6.
[c] Column 2a, metasediment fluid, forward calculated (see text), and assuming no Pb/LILE fractionation during sediment dehydration (= "maximum sediment fluid").
[d] Column 2b, metabasalt fluid, by mass balance, from column 1 and column 2a (= "minimum crust fluid"). No Pb/LILE fractionation during sediment dehydration.
[e] Colmun 2c, percentage of element contributed from metabasalt fluid to composite fluid. No Pb/LILE fractionation during sediment dehydration.
[f] Column 2d, percentage of element contributed from metabasalt fluid to Izu VF magma. No Pb/LILE fractionation during sediment dehydration.
[g] Column 3a, metasediment fluid, forward calculated (see text), and using the corrected D's based on the 650° experiments of *Johnson and Plank* [1999]. Pb/LILE fractionation from 650° experiment (JP99).
[h] Column 3b, metabasalt fluid, by mass balance, from column 1 and column 2a. Pb/LILE fractionation from 650° experiment (JP99).
[i] Column 3c, percentage of element contributed from metabasalt fluid to composite fluid. Pb/LILE fractionation from 650° experiment (JP99).
[j] Column 3d, percentage of element contributed from metabasalt fluid to Izu VF magma. Pb/LILE fractionation from 650° experiment (JP99).
[k] Column 4a, metasediment fluid, forward calculated (see text), and using the corrected D's based on the 700° experiments of *Johnson and Plank* [1999]. Pb/LILE fractionation from 700° experiments (JP99).
[l] Column 4b, metabasalt fluid, by mass balance, from column 1 and column 3a. Pb/LILE fractionation from 700° experiments (JP99).
[m] Column 4c, percentage of element contributed from metabasalt fluid to composite fluid. Pb/LILE fractionation from 700° experiments (JP99).
[n] Column 4d, percentage of element contributed from metabasalt fluid to Izu VF magma. Pb/LILE fractionation from 700° experiments (JP99).

sediment (Ba ~830 ppm; Plank and Kelley, manuscript in preparation, 2003). Thus the sediment appears to control the Ba outflux at the Izu VF. This is somewhat surprising in the light of the results of other workers who suggest the metabasalt as significant source of Ba in arcs [e.g., *Plank and Langmuir*, 1993; *Brenan et al.*, 1995a; *Elliott et al.*, 1997; *Turner et al.*, 1998; *Class et al.*, 2000; *Dorendorf et al.*, 2000]. Further, fluid partitioning experiments indicate Ba transport from basaltic protoliths [e.g., *Keppler*, 1996; *Kogiso et al.*, 1997] (Figure 11). In view of the uncertainties associated with the partition coefficients, however, it remains uncertain at the present whether the metabasalt Ba is entirely absent at the Izu VF, or whether a very low metabasalt Ba was concealed by the metasediment fluid.

[38] With the possible exception of Ba, the pattern of the metabasalt fluids has key features of the typical "arc signature." The implication is that the metabasalt fluid alone could be responsible for imprinting an arc-like signature on the arc crust without a recycled sediment component being required. In the presence of metabasalt fluids only, however, the amount of element transfer and recycling in arc genesis would clearly be much lower. Hence once the eroded upper continental crust (that is reflected in global subducting sediment [*Plank and Langmuir*, 1998]) became available in subduc-

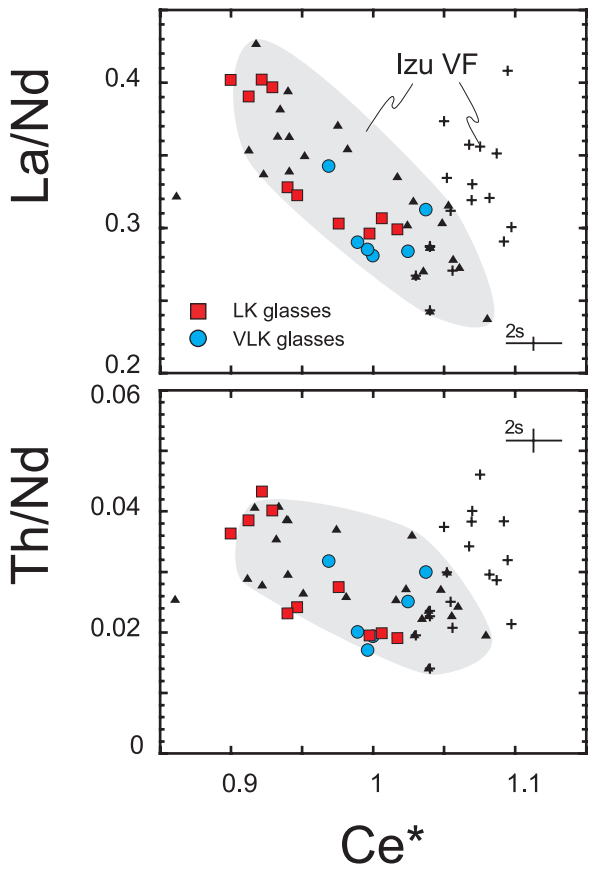

Figure 15. Ce/Ce* versus La/Nd and Th/Nd for the VLK glasses (blue circles) and LK (red squares). Ce/Ce* is the ratio of the measured Ce concentrations over the expected Ce* concentration, calculated from interpolation of the chondrite-normalized abundances of its rare element neighbors. Filled triangles, central; Izu VF volcanoes Sofugan, Sumisu-jima, Torishima and Hachijojima; Crosses, Izu VF volcanoes Mikayejima, Oshima and Aogashima in the Northern Izu arc. Izu VF data are from *Taylor and Nesbitt* [1998] and *Langmuir et al.* [2004].

tion zones, it should exert a significant control on the magnitude and the chemical signature of the arc outflux [e.g., *Plank and Langmuir*, 1993, 1998; *Patino et al.*, 2000].

4.3. Recycling Efficiency of Fluids and Partial Melts

[39] There are three aspects of the slab fluid calculation that we have carried out that we find particularly significant: (1) the calculations are based on glass compositions that illustrate simple systematics; (2) they are made in an arc with isotopic and other evidence for a minimal sediment contribution, and therefore the fluid component is relatively well constrained; (3) the fluid compositions have been remarkably constant over a fifteen million year time period.

[40] Although there are significant uncertainties to the calculations, these unique aspects suggest that this fluid composition is both well determined and remarkably robust. Therefore while additional refinements will occur as experimental data for fluid/rock partitioning improve, it is nonetheless worthwhile to explore some possible inferences that this fluid composition may have for arc volcanism at other convergent margins.

[41] Our approach is to assume that the arc fluid consists of two components, one from sediment and the other from the subducting basalt. The basalt component is likely to be similar from one arc to the other, since the basaltic portion of the oceanic crust varies little in comparison to the very large variations that exist in sediments. The sediment component must vary with subducting sediment composition. We therefore adjust the sediment fluid component for each element by multiplying the Izu sediment fluid composition by the ratio of trench sediment for the arc in question divided by the Izu trench sediment. Using these fluid compositions we can then explore what constraints they provide on the NON-fluid contributions that many have proposed to be present at other arcs.

[42] We consider the Aleutians (exemplified by the island of Umnak) and the central Marianas arc in order to make the comparison straightforward. Both of these, like the Izu arc, are oceanic islands built on crust that is neither thick nor continental, and appear to be derived by similar extents of melting [*Plank and Langmuir*, 1988; *Hochstaedter et al.*, 2000; *Miller et al.*, 1992], as indicated by the fairly similar HREE abudances. All three arcs have relatively complete and recent data sets [*Miller et al.*, 1992; *Elliott et al.*, 1997; *Class et al.*, 2000; *Hochstaedter et al.*, 2000, 2001]. Like the Izu VF, Umnak and the Marianas also have low-K to medium-K arc basalts to dacites with basaltic andesites and andesitic compositions being most abundant [*Miller et al.*, 1992; *Elliott et al.*, 1997].

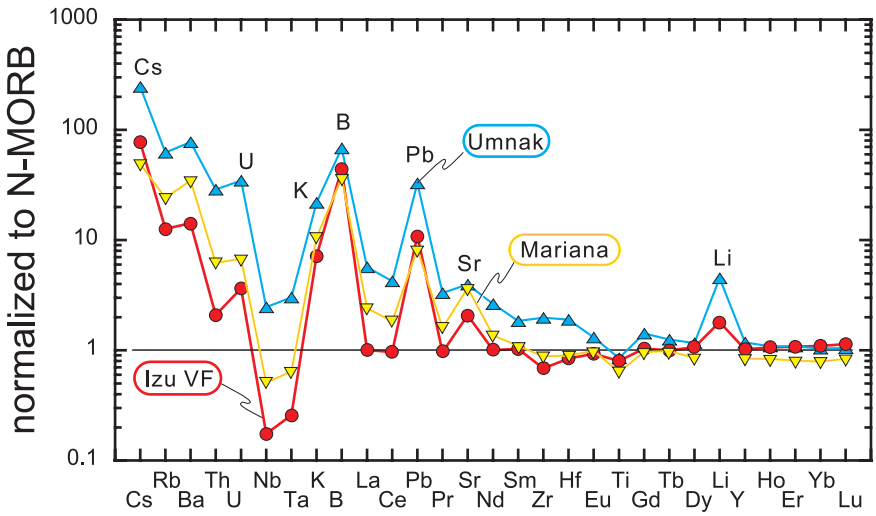

Figure 16. Averaged abundances of incompatible trace elements of the Izu VF (red filled circle), Mariana (yellow inverted triangles) and Umnak lavas (blue triangles). (Data are from *Taylor and Nesbitt* [1998]; *Langmuir et al.* [2004]; *Elliott et al.* [1997], *Class et al.* [2000]). The Ta data the Izu VF lavas are calculated using on the Nb of *Taylor and Nesbitt* [1998] and the average Ta/Nb of the Izu tephra glasses.

Further, the mantle wedge consists of more or less depleted N-MORB source in all three settings [*Elliott et al.*, 1997; *Class et al.*, 2000; *Hochstaedter et al.*, 2000]. Despite of these common features, Figure 16 shows that the abundances of the highly incompatible trace elements vary by one order of magnitude between the three arc settings with the Izu VF and Umnak being least and most enriched. The variation includes fluid-immobile elements such as Nb, Th and LREE. Note that the gross interarc differences are not sensitive to the along-arc geochemical heterogeneities that are well-establihed within the individual arcs considered here (Izu VF, central Marianas, and eastern Aleutians [e.g., *Taylor and Nesbitt*, 1998; *Notsu et al.*, 1983; *Kay and Kay*, 1994; *Elliott et al.*, 1997]). In the following, we will explore what the enrichments in the Umnak and Mariana mantle sources relative to the Izu VF may reveal about sediment contributions and subduction processes. These questions have also been extensively discussed in the primary papers that dealt with these arcs [e.g., *Kay and Mahlburg-Kay*, 1988; *Miller et al.*, 1992; *Class et al.*, 2000; *Elliott et al.*, 1997].

4.3.1. Calculation of the Fluid Fluxes

[43] A simple method to test for the presence and nature of non-fluid sediment additions in the mantle source is to substract the composition of composite fluid plus background mantle from the total arc source (sum of background mantle plus composite fluid plus sediment component). The residual patterns should be enriched in fluid-immobile elements typically transported in sediment melts (e.g., Th, LREE), and, if a bulk sediment component was added rather than a partial sediment melt, should be similar to the trench sediment.

[44] The Umnak background magma corresponds to average N-MORB [*Class et al.*, 2000]. A Mariana background magma was calculated assuming that the average Nb, Ta and HREE abundances of the *Elliott et al.* [1997] Mariana samples are entirely mantle-derived, and then following the procedures outlined in appendix A2.2. The Umnak and Mariana background mantle sources were calculated as described in appendix A2.3. The compositions of the Umnak and Mariana background magmas and mantle sources are given in Tables 8 and 9. The compositions of the Mariana and Umnak composite fluids were obtained building on two assumptions: (1) the metabasalt fluid flux is similar in all arcs, since similarly thick, mature Pacific MORB is subducted in all three settings (at this point, we disregarded the enriched alkaline basalts subducted beneath the Marianas), and (2) the metasediment fluid is only affected by the composition of the trench sediment whereby the effects of the convergence rate, the sediment

Table 8. Composition of Umnak Trench Sediments, Umnak Magmas and Mantle Sources and Components (for Details of Calculation See Text)[a]

	1	2	3	4	5	6a	6b	6c	7a	7b	7c
						Okmok 87-06-01			Recheshnoi lum 20		
	Trench Sediment[b]	Lower Trench Sediment[c]	Background Mantle[d]	Umnak Composite Fluid (Bulk Trench Sed.)[e]	Umnak Composite Fluid (lower Trench Sed.)[f]	Magma[g]	Mantle Source[h]	Residual Comp.[i]	Magma[g]	Mantle Source[h]	Residual Comp.[i]
Cs	3.4	4.1	0.0014	3.8	4.0	2.403	0.481	0.399	4.697	0.941	0.859
Rb	57	67	0.11	44	48	35.98	7.2	6.13	70.68	14.2	13.08
Ba	2074	732	1.3	1454	513	448	89.7	78.2	735	147.2	135.7
Th	5.46	6.67	0.024	1.21	1.40	3.11	0.62	0.572	5.63	1.13	1.077
U	2.39	2.78	0.009	1.27	1.39	1.51	0.30	0.266	2.82	0.57	0.529
Nb	7.7	10	0.468	0	0	5.51	1.11	0.648	6.4	1.29	0.827
Ta	0.55	0.69	0.027	0	0	0.38	0.08	0.050	0.47	0.09	0.068
K	17506	20772	122	26225	27477	11372	2309	1640	20419	4146	3477
La	18.0	21.1	0.51	2.9	3.3	13.29	2.7	2.16	17.85	3.7	3.09
Ce	39.0	43.3	1.59	6.2	6.9	31.58	6.68	4.99	39.21	8.29	6.60
Pb	12.9	15.7	0.07	19.2	21.5	10.49	2.35	1.86	13.37	3.00	2.50
Sr	245	228	20	1466	1450	351	76	28.1	273	59	11.1
Nd	19.1	21.4	1.637	2.9	3.3	20.56	4.6	2.94	22.1	5.0	3.29
Sm	4.43	4.69	0.620	0.7	0.72	5.31	1.25	0.630	5.39	1.27	0.649

[a] All element values in ppm.
[b] Column 1: Umnak trench sediment from *Plank and Langmuir* [1998].
[c] Column 2: Lower Umnak trench sediment (25% green clay, 75% clastic turbidites) after *Plank and Langmuir* [1998].
[d] Column 3: Umnak background mantle, assuming average N-MORB as background magma, see text for calculation.
[e] Column 4: Umnak composite fluid (5% Umnak sediment fluid plus 95% Izu metabasalt fluid), based on bulk trench sediment, see text for calculation.
[f] Column 5: Umnak composite fluid (5% Umnak sediment fluid plus 95% Izu metabasalt fluid), based on lower trench sediment, see text for calculation.
[g] Columns 6a and 7a: Two selected magma compositions of Umnak volcanoes Okmok and Recheshnoi are from *Class et al.* [2000].
[h] Columns 6b and 7b: Mantle source compositons are calculated assuming 20% batch melting, a depleted peridotite (OLIV:OPX:CPX = 60:25:15), and partition coefficients of column 9 in Table 7.
[i] Columns 6c and 7c: Residuals comp. are source composition minus a mixture of 2% Umnak composite fluid and 98% background mantle. The composition of the composite fluid is based on the composition of the lower Umnak trench sediment, whereby differences to composite fluid compositions based on the entire trench sediments are insignificant.

thickness and sediments density on the sediment outflux of the arcs are within 10% between the three settings and are hence negligible [*Plank and Langmuir*, 1993, 1998; *Plank et al.*, 2000]. Therefore the Mariana and Umnak composite fluids should differ from the Izu composite fluid only by the same factor their respective trench sediments differ.

[45] We used the average of the two forward calculated Izu metasediment fluids to represent the Izu metasediment fluid (average of columns 3a and 4a in Table 7). The Mariana and Umnak metasediment fluids were obtained by multiplying this Izu metasediment fluid by the same factor the compositions of the trench sediments differ. Mariana and Umnak composite fluids are then produced by adding five percent of the Mariana and Umnak metasediment fluids to the Izu metabasalt fluid. Two percent of these composite fluids were added to the Mariana and Umnak background mantle wedge, and the mixture substracted from the Mariana and Umnak mantle sources to obtain a ''residual component'' in the mantle source. Results are listed in Tables 8 and 9. The modeling results are insensitive to proportions of metasediment to metabasalt fluid, and proportion of composite fluid to wedge, for ratios commonly found in mixing models [*Hawkesworth et al.*, 1997; *Class et al.*, 2000; *Hochstaedter et al.*, 2001; *Ishizuka et al.*, 2003]. These are proportions of up to 10% metasediment fluid in composite fluid, and up to 5% composite fluid in the wedge.

4.3.2. Signatures of Residual Components in the Mariana and Umnak Sources

[46] Figures 17 and 18 compare the residual source components (blue) for selected lavas of the Umnak and Mariana arcs with the trench sediment patterns

Table 9. Composition of Mariana Trench Sediment, Mariana Magmas and Mantle Sources and Components (for Details of Calculation See Text)[a]

1	2	3	4a	4b	4c	5a	5b	5c	6a	6b	6c	
				Guguan 11			Agrigan 8B			Uracas 6		
	Trench Sediment[b]	Background Mantle[c]	Mariana Composite Fluid[d]	Magma[e]	Mantle Source[f]	Residual Comp.[g]	Magma[e]	Mantle Source[f]	Residual Comp.[g]	Magma[e]	Mantle Source[f]	Residual Comp.[g]
Cs	1.32	0.0007	3.1	0.271	0.054	0.004	0.463	0.093	0.043	0.675	0.135	0.085
Rb	30	0.057	32	7.2	1.44	0.87	19.9	4.0	3.42	18.3	3.7	3.10
Ba	311	0.64	218	190	38.1	33.9	165	33.0	28.9	424	84.9	80.8
Th	2.6	0.012	0.78	0.297	0.060	0.035	0.894	0.18	0.155	1.501	0.30	0.276
U	0.58	0.0048	0.67	0.175	0.035	0.020	0.377	0.08	0.060	0.511	0.10	0.087
Nb	11.0	0.24	0	0.7	0.14	−0.095	1.13	0.23	−0.008	2.11	0.42	0.188
Ta	0.76	0.017	0	0.069	0.014	−0.003	0.088	0.02	0.001	0.143	0.03	0.012
K	11270	89	23835	4233	859	391	7387	1500	1031	8384	1702	1233
La	20.8	0.42	3.3	3.18	0.65	0.19	7.45	1.5	1.07	10.05	2.1	1.60
Ce	31.5	1.45	5.1	8.53	1.80	0.30	15.76	3.33	1.82	22.2	4.69	3.19
Pb	6.0	0.062	13.4	2.44	0.55	0.27	1.79	0.40	0.13	4.23	0.95	0.67
Sr	161	18.1	1387	306	66	26	395	86	45.8	319	69	29.3
Nd	21.0	1.53	3.2	7.47	1.68	0.120	10.73	2.4	0.85	14.92	3.3	1.79
Sm	4.6	0.57	0.71	2.43	0.57	−0.001	2.79	0.66	0.084	4.3	1.01	0.441

[a] All element values in ppm.
[b] Column 1: Mariana trench sediment from *Plank and Langmuir* [1998].
[c] Column 2: Mariana background mantle, see text for calculation.
[d] Column 3: Mariana composite fluid (5% Mariana sediment fluid plus 95% Izu metabasalt fluid), see text for calculation.
[e] Columns 4a, 5a, 6a: Three selected magma compositions from *Elliott et al.* [1997].
[f] Columns 4b, 5b, 6b: Mantle source compositons are calculated assuming 20% batch melting, a depleted peridotite source (OLIV:OPX:CPX = 60:25:15), and bulk partition coefficients of column 9 in Table 7.
[g] Columns 4c, 5c, 6c: Residuals comp. are source composition minus a mixture of 2% Mariana composite fluid and 98% background mantle. Negative values indicate effectively zero abundance of element in residual comp.

(brown). The residual component in the Umnak source matches closely the signature of the trench sediments except for the Ba excess shown by the trench sediment (left hand side of Figure 17). The close match of the other elements, including the fluid-immobile Th, Nb, Ta and the LREE, suggest that the Umnak residuals represented the moderately fractionated sediment melt component that is present in the source of Umnak [*Class et al.*, 2000]. Interestingly, the fit between residual component and trench sediment is much improved if Ba was lost from the trench sediment prior to the arc front. Massive fluid loss of Ba by as much as two-third, however, is unlikely, given the only moderate loss of the more fluid-mobile Cs from the sediment trenchward to the Umnak arc [*Class et al.*, 2000] (Figure 19c). Because the eastern Aleutians are an accretionary margin [*von Huene and Scholl*, 1991], a more likely cause for substantial Ba loss was partial accretion of the trench sediment. The excursively high Ba of the Umnak trench sediment (Ba = 2074 ppm compared to the global average of Ba = 776 ppm in marine sediments [*Plank and Langmuir*, 1998]) results from the Ba-rich diatom oozes that make up the upper half of the trench sediment [*Plank and Langmuir*, 1998]. The diatom oozes are depleted in all other elements except for Ba, so that its loss from the sediment column lowers Ba substantially without much effect on the other elements. The lower trench sediment, consisting of 25% clay and 75% clastic turbidites, has an average Ba of 732 ppm (Table 8), and shows an improved fit with the source residuals (right hand side in Figure 17).

[47] The residual patterns in the Mariana mantle sources are more ambiguous. None of the residuals, including those of the sediment melt-bearing Mariana end-members (Agrigan, Uracas), matches the pattern of the Mariana trench sediment. In particular, the Nb-Ta anomaly of the Mariana trench sediment is not reproduced, pointing to no, or very minor, Nb and Ta transfer from the slab. On the other hand, the Agrigan and Uracas residuals show partial coincidence of Th and the LREE with the trench sediment pattern. These signatures might

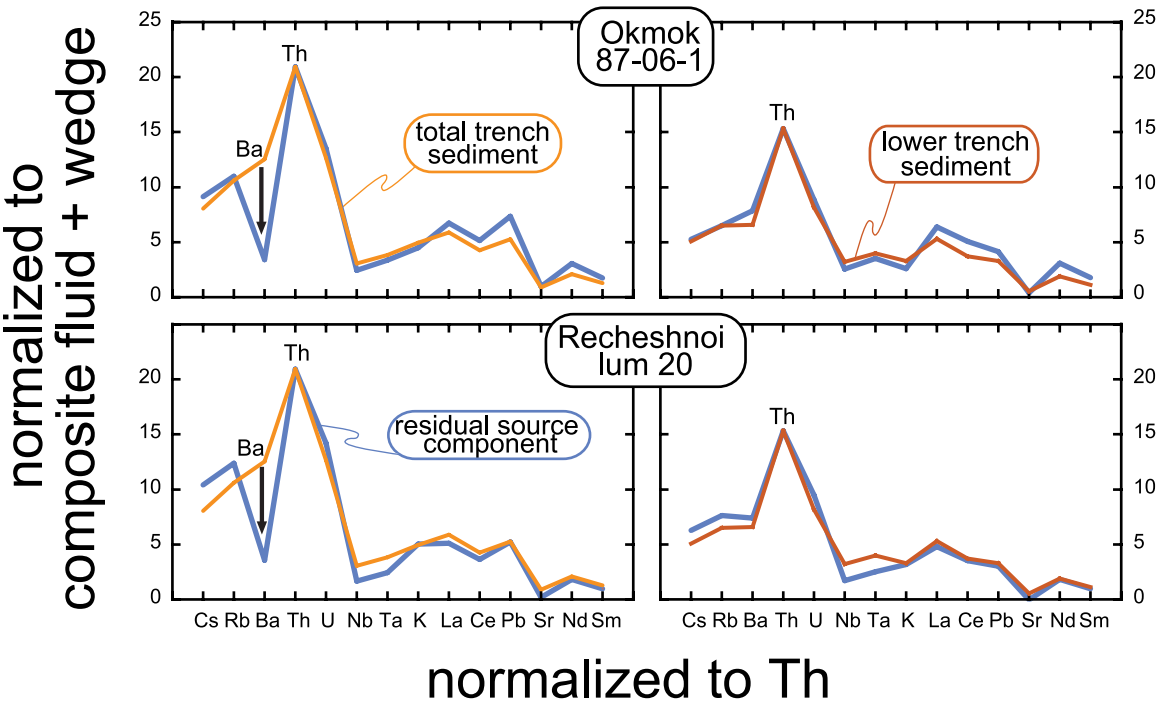

Figure 17. The residual components (blue) in the sources of two Umnak lavas from *Class et al.* [2000]. The data are normalized to Th and divided by a mixture of 98% mantle wedge and 2% Umnak composite fluid listed in Table 8. Light brown line on the lefthand side is based entire trench sediment column [*Plank and Langmuir*, 1998]. Note improved fit of trench sediment with arc source residual, if the lower trench sediment (brown line on right hand side) only is used (a mixture of 75% clastic turbitdites and 25% green clay from *Plank and Langmuir* [1998]), assuming that the upper Ba-rich diatom oozes has been accreted at the trench.

be explained if a fractionated, partial sediment melt component was present in the source of some Mariana volcanoes. The partial sediment transports primarily Th and LREE, while Nb and Ta were mostly retained by residual rutile in the slab [*Hawkesworth et al.*, 1997; *Elliott et al.*, 1997; *Turner et al.*, 1998]. While this might explain the signatures of the fluid-immobile elements, partial sediment melt addition does not account for the high Ba/Th ratios of the Mariana residuals, since these element do not fractionate during sediment melting [*Johnson and Plank*, 1999]. Rather, the excess Ba enrichment, that is sometimes coupled by minor enrichments of other fluid-mobile LILE, suggests an additional fluid source that is not accounted for by the slab sources so far considered. The most likely source for the excess Ba is the subducting metabasalt that is interpersed with alkaline basalts outboard the Marianas [*Kelley et al.*, 2003]. The persistent Ba excess in the residuals is consistent with the observation that Ba is the only fluid-mobile elements that is strongly enriched in the alkaline crust relative to the altered tholeiitic crust (by a factor of 23) while the other fluid-mobile elements Cs, Rb, K, Pb and Sr are much less enriched (by factors of 2–4). Therefore the Mariana residuals may tentatively be interpreted as representing either an fluid component from an enriched metabasalt source (Guguan source) or partial sediment melt components that are overprinted by metabasalt fluids from an enriched, alkaline crust (Agrigan, Uracas sources).

4.3.3. A Working Model

[48] To summarize, the interarc comparison suggests that the Izu VF and Umnak arc represent two extremes of the spectrum: the relatively depleted Izu VF that has only slab fluids in source, and the highly enriched Umnak arc that has a moderately fractionated sediment component in source next to the slab fluids. The relation between arc enrichment and slab component clearly suggests that the mode of transport (fluid versus melt) from slab substantially influences the arc chemistry. If slab fluids had low

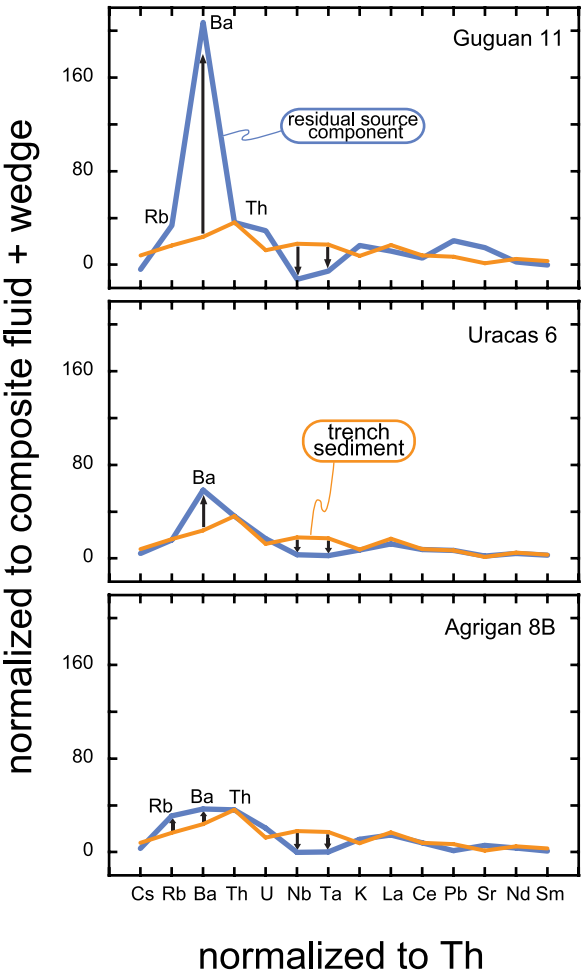

Figure 18. The residual components (blue) in the sources of three Mariana lavas from *Elliott et al.* [1997]. The data are normalized to Th and divided by a mixture of 98% mantle wedge and 2% Mariana composite fluid listed in Table 9. Upward arrows indicate element gain by an additional component (fluid from enriched alkaline metabasalt?), downward arrows indicate Nb and Ta retention in slab, presumably by residual rutile.

transport capacities for slab-derived elements, while that of the sediment melts was high, the contrasting abundances of the Izu VF and Umnak arcs can be explained without calling upon additional source components. The suggested role of the tranport agent also explains the intermediate enrichment of the Mariana magmas, as mixed fluid-sediment melt signals whereby the contributions of the partial sediment melt components are too small to suppress the signature of the comingling slab fluids.

[49] This model implies specific predictions regarding the influence of sediment melts on the arc chemistry that must be reflected in the observed arc data. If the influence of moderately fractionated sediment melts on the arc chemistry was so substantial, then the sediment-controlled Umnak arc (and other sediment melt-controlled arcs) should have LILE/HFSE ratios similar to the trench sediment. In contrast, the fluid-controlled Izu VF should have much higher LILE/HFSE ratios than the trench sediment. The Marianas should take an intermediate position, and display a range in the LILE/HFSE ratios that is bracketed by the Izu VF (maximum fluid fractionation) and the Mariana trench sediment.

4.3.4. Chemical Consequences of Fluid and Melt Recycling

[50] Figure 19 compares the LILE-Th systematics of the three arc settings to their trench sediments. Th was chosen as reference element, since Th is virtually immobile in fluids, but strongly enriched in sediment melt components [*Hawkesworth et al.*, 1997; *Johnson and Plank*, 1999]. Note that the full range of basalts to dacites and rhyolites in each arc is used, which emphasizes the variations inherited from the mantle relative to those induced by crustal differentiation.

[51] The effect of sediment melt and fluid recycling is best demonstrated in the Rb versus Th diagram, since the trench sediments have similar Rb/Th ~11 in all three settings. The Izu and Umnak trench sediments also have similar Rb and Th abundances. The three arcs, however, differ systematically in Rb and Th abundances and in Rb/Th ratios. At the Izu VF, Rb and Th abundances are lowest, and Rb/Th is highest (~28). The Aleutians are most enriched in Rb and Th, but have the lowest Rb/Th ratios (~11). The Marianas take an intermediate position in Rb/Th, while Rb and Th are only moderately higher than at the Izu VF. Clearly, the addition of a single sediment component does not account for the systematic differences between the arcs. However, the signatures can be explained if a low-Rb and low-Th fluid with high, fractionated Rb/Th was added to the Izu VF source, but a Rb- and Th-rich bulk sediment component was added to the Umnak source.

[52] While Rb is mobile in both fluids and melts, La is, as Th, mainly transported in sediment melts.

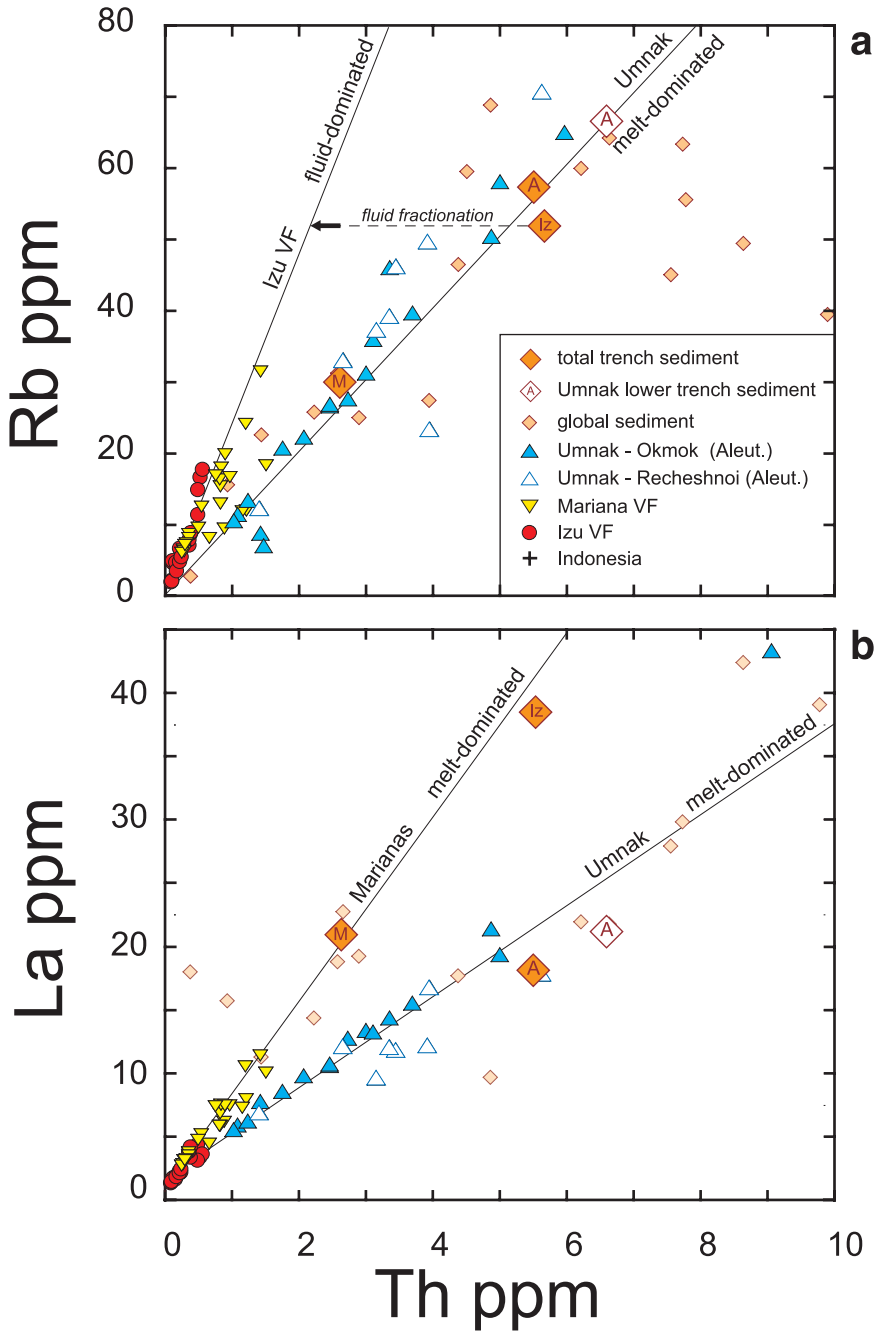

Figure 19. (a–b) Rb, La versus Th; (b–c) Cs, Pb versus Th, and (c) Ba, U versus Th for the Izu VF (red triangles, based on the Izu glasses), the Mariana VF (yellow inverted triangles), the western Aleutians (exemplified by Umnak volcano; blue open and closed triangles), and Indonesian arc (black crosses) compared to trench sediment (big brown diamonds). Small brown diamond indicate global trench sediment. Sediment data from *Plank and Langmuir* [1998]. Mariana data are from *Elliott et al.* [1997], Umnak data from *Miller et al.* [1992] and *Class et al.* [2000], Indonesia data from *Alves et al.* [1999] and *Turner and Foden* [2001]. For discussion see text.

Thus arcs with sediment melt components in source should show clear trends toward their trench sediments in La versus Th diagrams, and the arcs with a larger sediment melt contribution should be more enriched. Figure 19b shows that this prediction holds for the Umnak and Mariana arcs. As expected, the Izu VF is highly depleted in Th and La. Somewhat surprisingly, similar systematics

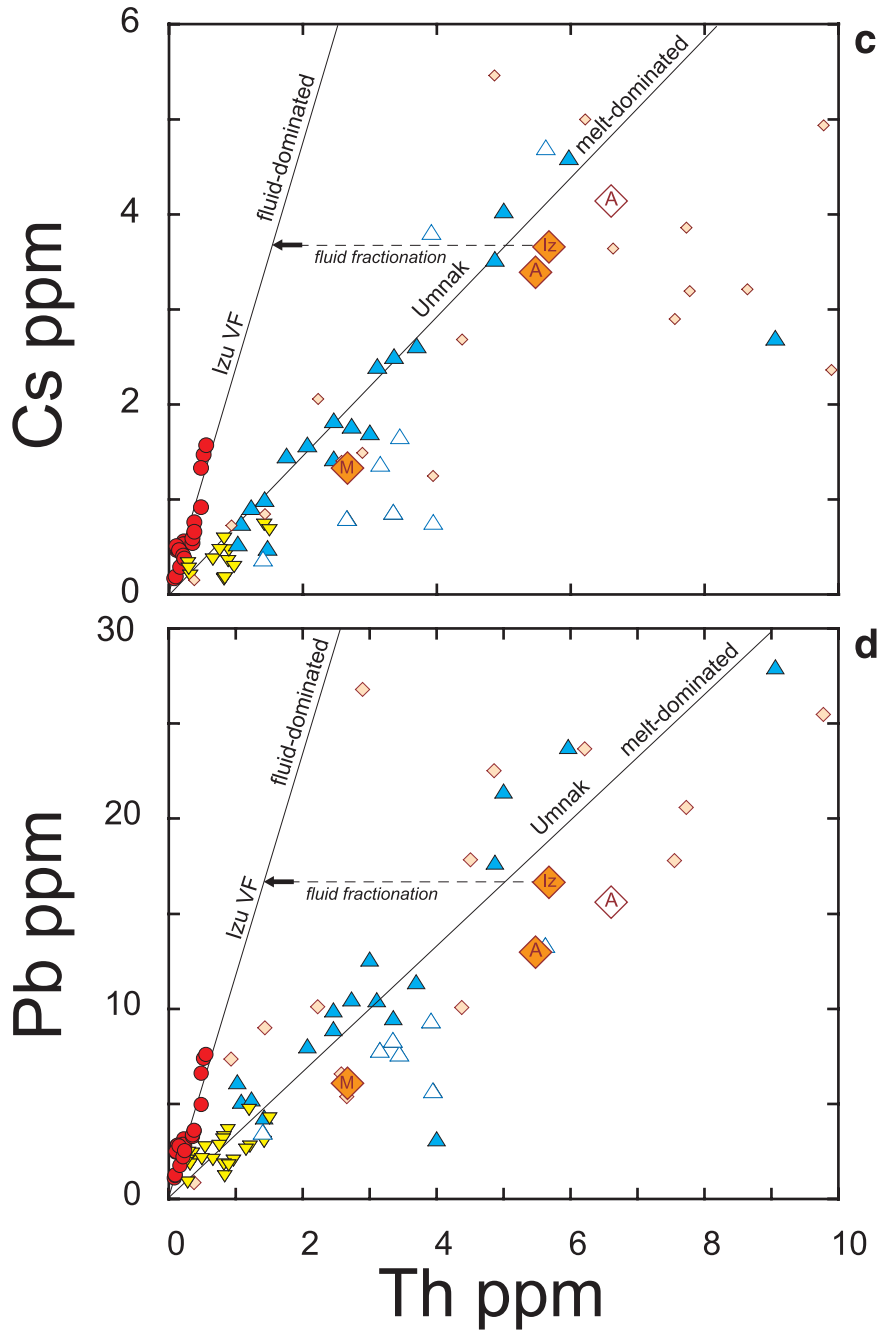

Figure 19. (continued)

between fluid- and sediment-controlled arcs also hold in diagrams that involve highly fluid-mobile elements such as Cs and Pb. These elements are conducive to loss during shallow slab dehydration [*Dorendorf et al.*, 2000; *Churikova et al.*, 2001; *Ryan et al.*, 2001], and thus their input into the arc sources may be reduced. Indeed, evidence for fluid-induced Cs loss has been found at Umnak volcano Recheshnoi [*Class et al.*, 2000]. Although Figures 19c and 19d show that Recheshnoi has systematically lower Cs and Pb abundances relative to Okmok, both volcanoes are still much more enriched than the Izu VF and the Marianas, and trend broadly toward the Cs/Th and Pb/Th of their trench sediments. This argues that, despite some fluid loss, the subducting sediment body remains largely intact until melting. Again, the much higher Cs/Th and Pb/Th ratios of the Izu VF relative to

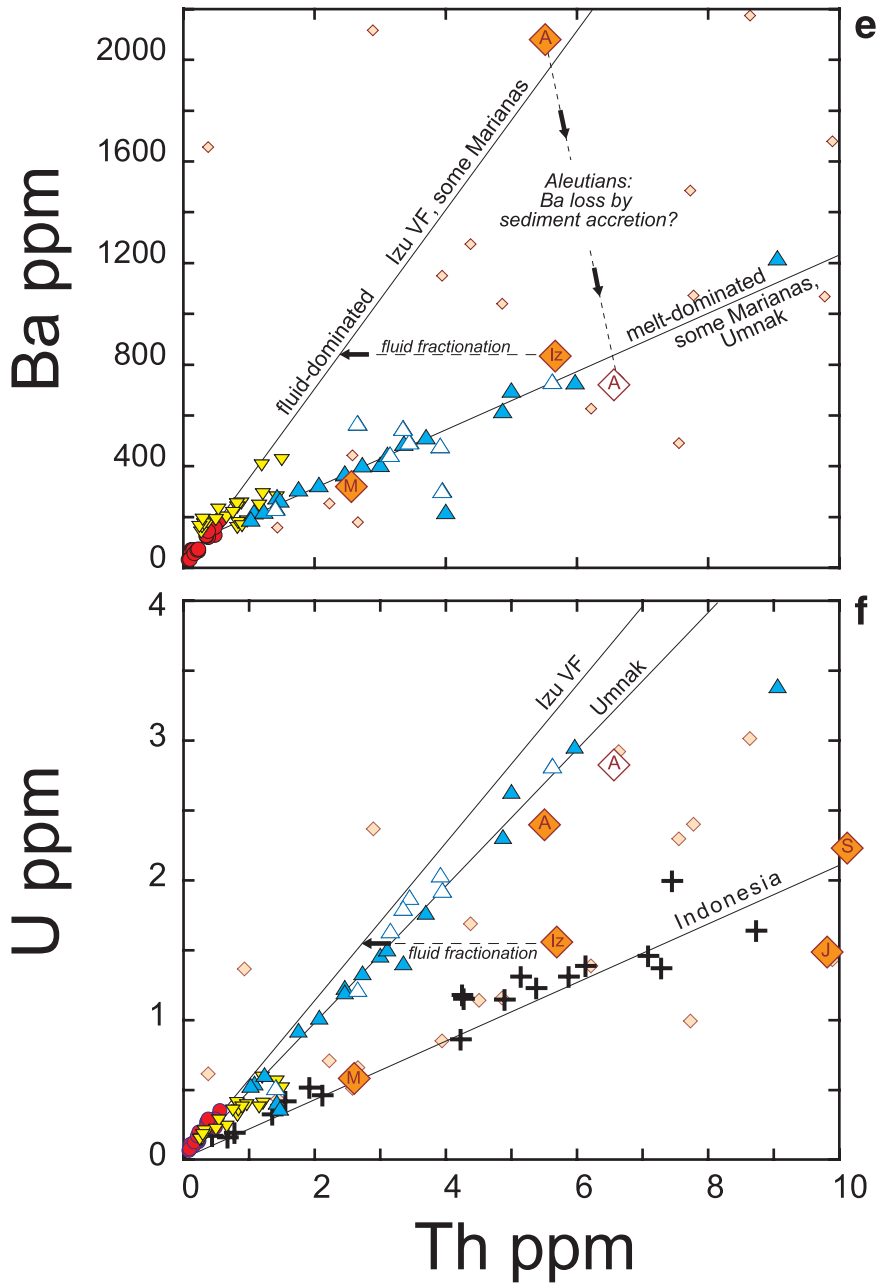

Figure 19. (continued)

trench sediment are consistent with the addition of a fractionated, relatively depleted fluid component to the Izu VF source.

[53] The lower recycling efficiency of slab fluids is further illustrated by the Ba-Th systematics (Figure 19e). (Note that the Umnak lavas trend to the Ba/Th ratio of the lower trench sediment only, consistent with the presumed removal of the Ba-rich oozes at the trench.) Even if some Mariana arc lavas trend toward the trench sediment, others have higher Ba/Th ratios relative to trench sediment, consistent with addition of extra Ba from slab fluids and consequently a higher Ba/Th of the total slab component. Despite of this fluid addition of Ba, however, the Ba abundances of the Mariana arc remain substantially lower than Umnak.

[54] The Th-U systematics suggest that the fluid-mobile U was more efficiently recycled by sediment melts than by fluids (Figure 19f). The dependency of sediment-controlled arcs on the U/Th of the

trench sediment is testable, since the U/Th of trenchsediments varies widely on a global scale consequent to the variable behaviour of U under oxidizing conditions on the Earth's surface [*Plank and Langmuir*, 1998]. As expected, the high U/Th of the Umnak lavas is associated with high-U/Th trench sediments (Figure 19f). In contrast, the U- and Th-rich, sediment melt-controlled Java and Sumatran arc lavas trend toward the low U/Th of the Indonesian trench sediments. Again, the Marianas take an ambiguous position, with the U- and Th-poorer Mariana samples having higher U/Th ratios than the U- and Th-richer Mariana lavas which have the lower U/Th ratios of the Mariana trench sediment. A moderate U mobility in fluids relative to sediment melts also provides an explanation for the apparent absence of ^{238}U excesses in some arcs. This is because ^{238}U excess of the slab fluids should be masked by a comingling sediment melt, which is rich in U and Th, and equilibrated. Such "masking" would explain (1) why the fluid-controlled Mariana lavas with the lowest U/Nb, and lowest U and Th abundances (e.g., Guguan) have the highest ^{238}U excess, whereas the ^{238}U excess is small to non-existent in the sediment-rich end-member (Agrigan) with high Th and U contents [*Elliott et al.*, 1997], and (2) why U/Nb is cocorrelated with Th/Nb in the Marianas lavas [*Elliott et al.*, 1997, Figure 8c]. An analogue observation can be made for the Indonesian arc, where the ^{238}U excesses are confined to the depleted, fluid-controlled arc front lavas. Therefore consistent with the observations of *Hawkesworth et al.* [1997] we would expect that measurable ^{238}U excess were confined to arc magmas that have little or no sediment melt component in source, and a relatively depleted mantle wedge. Further, if Th and U are not fractionated during sediment addition to source, our model implies that the ascent rates of magmas with sediment melt components in source are virtually unconstrained, and that fluid and sediment melt components could possible be transferred at similar timescales (~100 to 1000 yrs) from slab to crust.

4.3.5. Summary

[55] In summary, our model confirms the strong dependencies of the arc chemistry on trench sediment that have been proposed by *Plank and Langmuir* [1993], in particular for arcs with sediment melt components in source. This strong link is enforced by (i) the grossly increased transport capacities of sediment melts relative to slab fluids, and (ii) the lack of fractionation of many LILE (e.g., Cs, Rb, Ba, U, Th, Pb) during sediment addition to source. In contrast, the lower transport capacity of fluids, coupled with LILE fractionation and mixing with metacrust fluids, should weaken this link. Clearly, the influence of the transport agent must affect the arc chemistry on a global scale. First, if the sediment melt-dominated arcs inherit the LILE/LILE ratios of the trench sediment, the Earth's surface processes must eventually influence the compositional diversity of arcs. Since the sediment volume and diversity evolve with time, from early pre-dominant volcaniclastic to an assemblage of volcaniclastic, detrital and pelagic sediments, the arc chemistry should reflect this evolution. Second, the isotopic evolution of the crust, and by subduction, of the Earth's mantle must be affected, since different fractionation patterns of many elements with radioactive isotopes exist for fluid-dominated and sediment melt-dominated arcs.

5. Conclusions

[56] The following are the conclusions of this study.

[57] 1. The Izu VF mantle source is fluxed by a slab-derived fluid that carries Cs, B, Ba, Rb, K, U, Pb, Th, Sr, La and Li and has high LILE/Th and LILE/U ratios relative to source.

[58] 2. The isotopic and elemental variability of the Izu VF fluids apparently reflect the variable amounts of total slab fluid added to the mantle wedge (~0.8 to ~3.7%; average ~1.6%).

[59] 3. The slab fluid is a composite fluid, with components from the metasediment (~5% of composite fluid) and the metabasalt (~95%). The metabasalt fluid is much less enriched but its large relative proportions make it an important carrier of Sr, Pb and K to the Izu VF.

[60] 4. The metabasalt fluid has the characteristics of the arc trace element signature with the possible

exception of Ba. Hence the presence of sediment components is not required to create the typical element pattern of arc volcanic rocks.

[61] 5. Partial melts of the subducted sediment are much more enriched than any slab-derived fluid, implying that recycling via sediment melts is much more efficient, and that the fluid signature can be suppressed in the presence of sediment melt components.

[62] 6. Slab-derived sediment melt components may impart a trace element signature to arcs that has been shaped by the processes on the Earth's surface. Since the sediment volume and diversity increase with time, sediment melt recycling should play a major role in the progressive differentiation of silicate Earth.

Appendix A: Elemental and Isotopic Composition of Source Components and Mixing Ratios at the Izu Arc Volcanic Front

A1. Pb Abundances and Pb Isotopic Composition of the Slab Fluids

[63] At the Izu VF, most of the Pb (~88–90%) and the Sr (~68%) originate from the subducting slab implying that the slab-derived Pb and Sr control the Pb and Sr isotope chemistry of the arc magmas [*Taylor and Nesbitt*, 1998; *Hochstaedter et al.*, 2001; *Schmidt*, 2001; *Ishizuka et al.*, 2003]. These authors also showed that Pb and Sr derive from both metasediment and the metabasalt fluids, forming a composite fluid, and that the volume of the metabasalt fluid is much larger (ranging between 99% and 88% in the various models) than that of the metasediment fluid. However, in spite of this general consensus, substantial disagreement consists in the various models concerning the trace element and isotopic composition of the end-members involved in the petrogenesis of the Izu arc front magmas. Therefore we repeated the modeling using the most recent end-member compositions available. The mixing ratios of the two slab fluids in the Izu VF source, as well as the mixing ratio of the wedge and composite slab fluid, were calculated using their Pb abundances and Pb isotope chemistry and the general mixing equation of *Langmuir et al.* [1978]. The Pb abundances and the isotope ratios for the three source components (metabasalt fluid, metasediment fluid, background mantle) were either compiled from the literature, or inferred from the observed data by inverse and forward approaches. All data are listed in Table 6. In short, the Pb abundances and the Pb isotope composition of the mixing end-member are similar to previous studies, except for the Pb isotope ratio of the wedge. Similar results were also obtained with respect to the proportions of metabasalt to metasediment fluids (~95%: ~5%), and the amount of composite fluid in Izu VF source (~0.8% to ~3.7%, average ~1.6%).

A1.1. Pb Chemistry of the Metabasalt Fluid

[64] The Mesozoic basement basalts of DSDP Sites 197, 303, 304 and 307 in the NW Pacific [*Janney and Castillo*, 1997] have an average Pb = 0.46 ppm (n = 8). The Pb content of the metabasalt fluid (Pb_{crust}^{fluid} = 8.7 ppm) was calculated using equation (3):

$$c_F = c_o/(D + F - DF) \quad (3)$$

whereby c_F = concentration in fluid, c_o = concentration in original solid, D = bulk solid/fluid partition coefficient (= sum of individual mineral/fluid partition coefficient K_ds), and F = amount of fluid released. We assumed (1) a fluid release of 0.25%, (2) an eclogite residuum of orthopyroxene:garnet in the proportions of 40:60, and (3) bulk mineral/fluid partition coefficient of D = 0.05 based on the partitioning data of *Brenan et al.* [1995a]. The results of this study are not affected if the protolith Pb ranged from 0.3 to 0.5 ppm Pb (corresponding to 5 and 10 ppm Pb in the metabasalt fluid). Since the Pb isotope ratios of the Mesozoic basalts are substantially changed by alteration [*Plank et al.*, 2000; *Hauff et al.*, 2003], the Pb isotope ratios of the metabasalt fluid were determined from the Pb versus Pb isotope diagrams. In Figure A1, the metabasalt fluid ("mbf") must lie on the backward extension of the mixing line between the metasediment fluid and the Izu VF tephras and lavas. The average mixing line merges with the Pacific N-MORB field

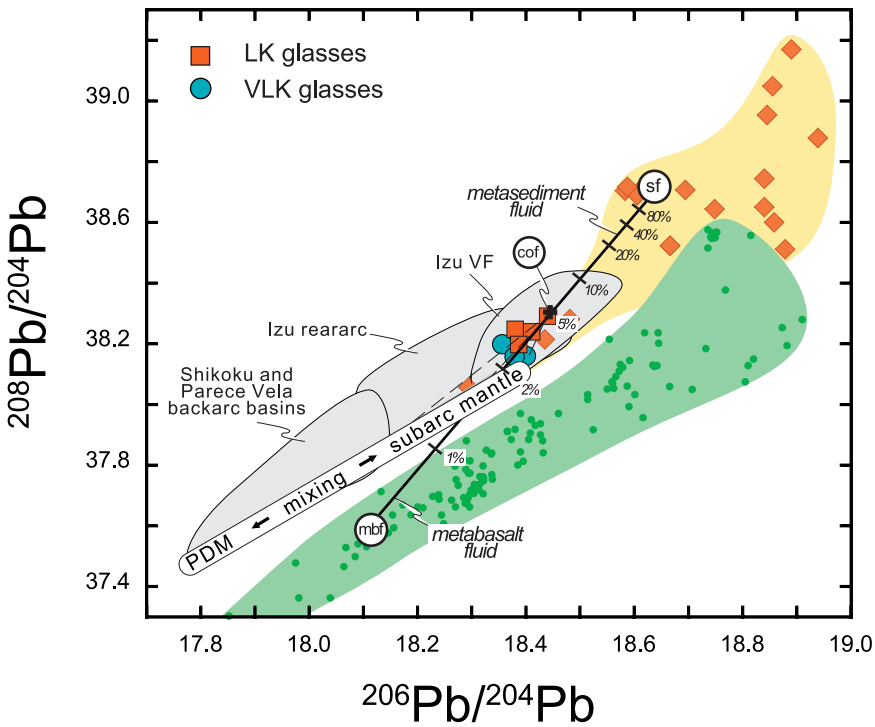

Figure A1. $^{208}Pb/^{204}Pb$ versus $^{206}Pb/^{204}Pb$ of Izu lavas from the arc front, the rear-arc and the Shikoku and Parece Vela backarc basins (fields outlined; data from *Taylor and Nesbitt* [1998]; *Langmuir et al.* [2004]; *Hochstaedter et al.* [2000, 2001]; *Ishizuka et al.* [2003]; *Hickey-Vargas* [1998]). The Izu VF glasses can be explained by adding a composite fluid (cof) to an isotopically heterogeneous mantle wedge that is a mixture of Philippine Depleted Mantle (PDM) and a subarc mantle component (white field). Thin stippled lines indicate potential mixing lines of composite fluid with background mantle. The composite fluid is a mixture of a metasediment fluid (sf) and a metabasalt fluid (mbf). Field of Pacific MORB is defined by data the East Pacific Rise spreading center (Petrological Database, http://petdb.ldeo.columbia.edu/petdb). See appendix for other data sources and details of modeling.

at approximately $^{206}Pb/^{204}Pb$ ~18.1 (Figure A1), and at $^{207}Pb/^{204}Pb$ ~15.44, $^{208}Pb/^{204}Pb$ ~37.6 (not shown).

A1.2. Pb Chemistry of the Metasediment Fluid

[65] The trace element composition of the Izu trench sediment is from *Plank and Kelley* [2003, manuscript in preparation, 2003]. The composition is the weighted average of 39 ICP-MS analyses of different lithologies of the trench sediment drilled at ODP Site 1149 outboard the Izu arc. The isotope compositions of the trench sediment was inferred from published isotope data of ODP Site 1149 pelagic clay (n = 4; 39% of total sediment) and radiolarite, porcellanite, chert, chalk and marl (n = 14, 56%) drilled in DSDP and ODP sites 195 198, 452, 800, 801 and 1149 in the NW Pacific [*Pearce et al.*, 1999; *Hochstaedter et al.*, 2001; *Hauff et al.*, 2003]. A small portion (5%) was allowed for arc-derived tephra (isotopic composition from *Schmidt* [2001]). The isotope composition of bulk sediment is: $^{206}Pb/^{204}Pb$ = 18.61, $^{207}Pb/^{204}Pb$ = 15.61 and $^{208}Pb/^{204}Pb$ = 38.64.

[66] The metasediment fluid Pb (Pb_{sed}^{fluid}) was calculated using equation (3). We assumed (1) a fluid release of 1%, and (2) the bulk Pb of the trench sediment as abundance of the original solid. The bulk mineral/fluid partition coefficient is difficult to constrain due to the current uncertainty of the $D_{sed/fl}^{Pb}$. At the given Pb = 16.7 ppm of the bulk sediment, the high $D_{sed/fl}^{Pb}$ (~0.6–0.9) of *Johnson and Plank* [1999] - that are compromised by experimental problems - results in Pb much too low in the composite fluid (~12 ppm Pb only). This amount cannot account for the total Pb content of the Izu VF at the given Pb of the metabasalt fluid. Therefore the $D_{sed/fl}^{Pb}$ = 0.05 of

Brenan et al. [1995a] was taken to calculate the Pb, assuming similar Pb_{sed}^{fluid} mobility during the dehydration of metasediment and metabasalt. For a 1% fluid release, the metasediment fluid has Pb_{sed}^{fluid} = 280 ppm.

A2. Pb Abundances and Pb Isotopic of the Izu VF Source and the Izu Background Mantle Wedge

[67] The trace element composition of the Izu VF source and the Izu VF background mantle were established using two Izu VF magma compositions. One magma composition is taken to represent an average primary Izu VF magma. The other magma composition is a hypothetical "background magma," i.e., a magma that would derive from the Izu VF background mantle without slab components. Since such "background magmas" do not exist, they have to be constructed.

A2.1. Composition of the Average Izu VF Magma

[68] The primary Izu VF magma average was inferred from the average of the basaltic andesitic glasses (samples 19, 29, 59, 94). Using the glasses avoids uncertainties that may be induced by the inherent HREE heterogeneity of the Izu mantle wedge. The basaltic andesitic glasses have only MgO ~4–5 wt%, but it is not clear how far they are evolved from their parental melts, given that broad spectrum of basaltic and andesitic melts is considered to be primary at the Izu VF [*Tamura and Tatsumi*, 2002]. Notably, the abundances of highly incompatible elements (among them Nb and Ta) in basaltic andesitic glasses and mafic lavas are very similar (Figure 3). This suggests that enrichment by fractional crystallization was minor in the glasses. If the most magnesium-rich Hachijojima basalt of MgO = 8.23 wt% was parental to the glasses, as little as ~20% crystallization of a cumulate of magnesian olivine (Fo_{89}; 30 vol%), clinopyroxene (mg# = 79; 20 vol%), orthopyroxene (mg# = 75; 20 vol%) and plagioclase (An_{90}; 30 vol%) is needed to produce the major element compositions of the basaltic andesitic glasses. Therefore the basaltic andesitic glasses were reduced by 20% in incompatible elements in order to ensure their comparability to the most primitive Izu magmas erupted.

A2.2. Composition of the Izu "Background Magma"

[69] The hypothetical Izu "background magma" was reconstructed based on three assumptions: (1) the Izu VF background mantle is more depleted than Indian MORB source [e.g., *Taylor and Nesbitt*, 1998; *Hochstaedter et al.*, 2001]; (2) mantle melting proceeds in similar fashions as beneath mid-ocean ridges, and therefore incompatible elements in these two different setting behave similarly during melting; and (3) the highly incompatible element Nb originates exclusively from the wedge, as consistent with its extremely low abundances (0.2 ppm) that are similar to the most depleted N-MORB known.

[70] Therefore Nb can be used in a simply way to determine which of the LILE are slab-derived. If the Nb-normalized ratio of a LILE is comparable to the ratio of highly depleted N-MORB, it was considered as wedge-derived. For example, the Yb/Nb ~8 of the Izu VF is similar to the Yb/Nb ~8 of MORB, all thus Izu VF Yb is considered to be wedge-derived. However, if LILE/Nb is higher than MORB, the element must have a slab contribution. For example, the La/Nb ~5.5–7 of the Izu VF is higher than highly depleted N-MORB (La/Nb ~ 3), indicating that some La derives from slab. Notably, no LILE/Nb of the Izu VF is lower than MORB, which supports the validity of this approach.

[71] Having identified all elements with slab additions, the composition of the background magma was calculated. To this purpose, it was assumed that the REE of the 'background magma" correspond to the average REE of the five most depleted East Pacific Rise MORB samples of *Niu and Batiza* [1997] that have identical HREE abundances as the fractionation-corrected basaltic andesitic glasses. The Nb and Ta of basaltic andesitic glasses, however, were taken to represent the contents of the background magma, as they are comparable to the most depleted MORB (Figure 10). Knowing, Nb, Ta and the REE of the background

magma, it's Sr, Pb, K and B (less incompatible than Nb) can be established by interpolating their abundances between the neighboring REE and HFSE, using the order of incompatibility of *Sun and McDonough* [1989]. Lastly, elements more incompatible than Nb (U, Th, Ba, Rb, Cs) were assumed to be similar depleted as Nb in the Izu VF source. Their abundances were calculated using the Izu VF Nb = 0.2 ppm, and their ratio to Nb as in average N-MORB of *Sun and McDonough* [1989].

A2.3. Abundances in the Izu Mantle Source

[72] The source abundances of the average Izu VF magma and background magma were calculated using a simple batch melting model, a degree of mantle melting of 20%, and a slightly depleted peridotite as source mantle (60% olivine, 25% orthopyroxene and 15% clinopyroxene). These numbers are based on of previous work [e.g., *Plank and Langmuir*, 1988; *Hochstaedter et al.*, 2000]. The bulk partition coefficients were calculated based on mineral/melt partition coefficients of *Donnelly* [2002] and are listed in column 9 of Table 6. A criterion for the validity of the inversion was whether sensible composition of the background mantle could be obtained, given the current knowledge of the compositions of oceanic depleted mantle [e.g., *Hofmann*, 1988; *Sobolev et al.*, 2000; *Donnelly*, 2002]). All the results are presented in Table 6.

A2.4. Isotopic Composition of the Izu VF Source and the Izu Background Mantle

[73] The isotopic composition of the Izu VF source is that of the Izu VF magmas. The isotopic composition of the Izu VF background mantle, however, is more difficult to establish since the mantle domain beneath the Neogene Izu arc is isotopically heterogeneous [*Taylor and Nesbitt*, 1998; *Hochstaedter et al.*, 2000, 2001; *Ishizuka et al.*, 2003]. Current models agree that Indian MORB source mantle (PDM, "Philippine Depleted Mantle") is present in the Izu wedge together with a second, isotopically different mantle domain [*Taylor and Nesbitt*, 1998; *Hochstaedter*, 2000, 2001; *Ishizuka et al.*, 2003]. Recently, *Ishizuka et al.* [2003] proposed that the Izu wedge is a mixture of these two mantle domains, that became infiltrated by fluids (Izu VF) and partial sediment melt components (Izu rear-arc) from slab. *Ishizuka et al.* [2003] suggested that the second mantle component was "Pacific MORB-like" and had the Pb isotopic ratios of average Pacific mid-ocean ridge basalts ($^{206}Pb/^{204}Pb$ = 18.35, $^{207}Pb/^{204}Pb$ = 15.48 and $^{208}Pb/^{204}Pb$ = 37.80).

[74] However, Pacific Pb isotope ratios for the second mantle component are not supported by the combined trace element and isotope systematics observed for Izu magmas. The Izu systematics are consistent with the existence of two mantle end-members, one of them being PDM. The second end-member, however appears to be isotopically similar to Indian MORB. The nature of this second component is illustrated in the $^{206}Pb/^{204}Pb$ isotope versus Nd/Pb diagram, where mixing lines are linear (Figure A2). Any slab fluids with a near-zero Nd/Pb (metabasalt fluid, metasediment fluid or composite fluid) must plot on the abscissa. Partial sediment melts also have low Nd/Pb (= 2.7; Plank and Kelley, manuscript in preparation, 2003) because Nd/Pb does not fractionate during melting [*Johnson and Plank*, 1999]. Therefore the Nd/Pb ratios >2.7 of the rear-arc lavas can only be generated by mixing with the background mantle that has high Nd/Pb ratios (~15 to ~25). In Figure A2, the unradiogenic PDM end-member is clearly identified by the trend of the Shikoku and Parece Vela backarc basin basalts, which are influenced by a subduction component. The second mantle end-member, defined by the trend of the Izu rear-arc magmas, is much more radiogenic, and has $^{206}Pb/^{204}Pb$ ~18.4 (and $^{207}Pb/^{204}Pb$ ~15.53 and $^{208}Pb/^{204}Pb$ ~38.20). Here, we term this component "subarc mantle" to avoid potential genetic implications that are beyond the scope of this paper. We note, however, that the isotopic composition of this subarc mantle is similar to that inferred by *Hochstaedter et al.* [2001] for the residual mantle beneath the western Izu rear-arc, which is also considered as potential background mantle for the Izu VF.

A3. Identifying the Source Components in the Izu VF Mantle Source

[75] The subhorizontal trend of the tephra glasses in the $^{206}Pb/^{204}Pb$ isotope versus Nd/Pb diagram

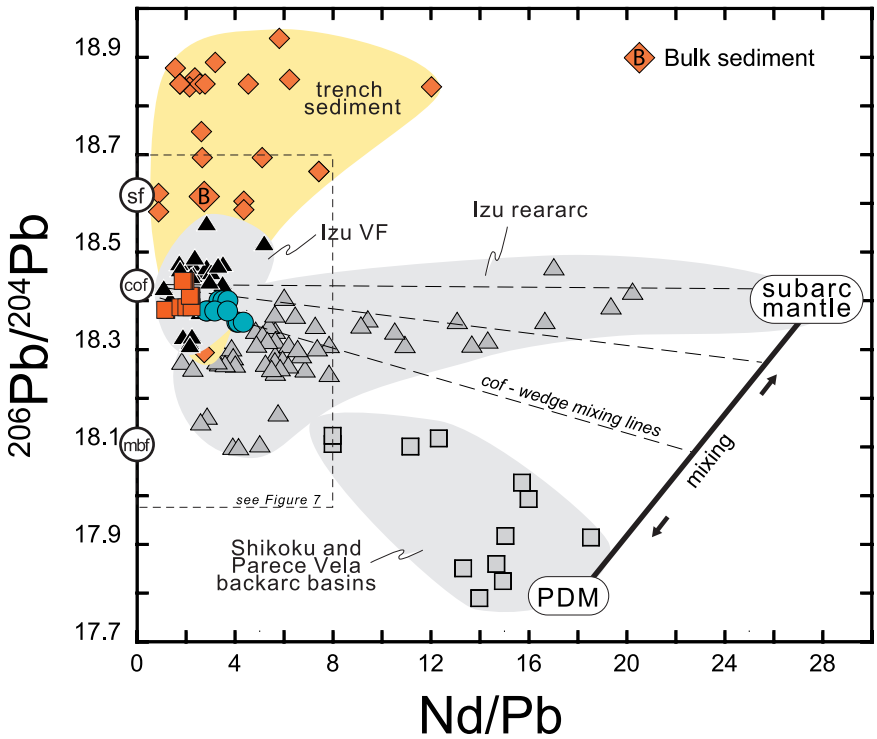

Figure A2. Nd/Pb versus $^{206}Pb/^{204}Pb$ isotope ratios for the Izu arc/backarc system. Data sources are as in Figure A1. The Izu VF magmas can be explained as a mixture of composite fluid (cof) with an isotopically heterogeneous mantle wedge that in turn is a mixture of Philippine Depleted Mantle (PDM) and a subarc mantle component (white field). sf metasediment fluid; mbf metabasalt fluid. See text for discussion. Details of modeling are shown in Figure 7.

intersects the y axis between $^{206}Pb/^{204}Pb$ ~18.33 and $^{206}Pb/^{204}Pb$ ~18.50, which is between the metasediment fluid ($^{206}Pb/^{204}Pb$~18.61, Nd/Pb~0) and the metabasalt fluid ($^{206}Pb/^{204}Pb$ ~ 18.1, Nd/Pb ~ 0) (Figure 7). Therefore the $^{206}Pb/^{204}Pb$ of the composite fluid is about ~18.42 (similar diagrams can be drawn for $^{207}Pb/^{204}Pb$ ~15.55 and $^{208}Pb/^{204}Pb$ ~38.31). In the absence of sediment melt component, the trend toward high Nd/Pb must point to the Pb isotopic composition of the background mantle. The tephra trends indicate isotopic ratios slightly less radiogenic than the subarc mantle (Figure A2; $^{206}Pb/^{204}Pb$ ~18.3, $^{207}Pb/^{204}Pb$ ~15.50 and $^{208}Pb/^{204}Pb$ ~38.0), consistent with the Izu VF background mantle being a mixture of PDM and subarc mantle domains.

A4. Mixing Ratios of Slab Fluids and Background Mantle

[76] The inherent heterogeneity of the background mantle and the slab components poses some problems with respect to adopting "average" end-members for the mixing calculations. Since the glasses cut through the field of the Izu VF lavas and record the last 15 million years, we suggest that their trends define best the average compositions of the composite fluid and the background mantle of the Neogene Izu VF. In all diagrams, an average composition of the trench sediment is shown, although the variability of the trench sediment is clearly reflected in the Izu arc magmas [e.g., *Ishizuka et al.*, 2003, *Plank et al.*, 2000]. The mixing proportions, however, are relatively insensitive to the isotopic variability of the end-member components.

[77] The mixing proportions of the two slab fluids were determined in the Pb versus Pb isotope diagram (Figure A1) and the $^{206}Pb/^{204}Pb$ isotope versus Pb/Nd diagram (Figure 7). Comparable to previous studies, the composite fluid was found to be a mixture of approximately 95% metabasalt fluid and 5% metasediment fluid. At this ratio, the composite fluid has Pb = 22.3 ppm, $^{206}Pb/^{204}Pb$ =

18.42, $^{207}Pb/^{204}Pb = 15.55$ and $^{208}Pb/^{204}Pb = 38.31$ (Table 6). On the basis of the mixing array defined by the VLK and LK glasses and the background mantle (Figure 7), the percentage of composite fluid in the source ranges from 0.8% to 3.7%, at an average of 1.6%. This is consistent with previous results: ~1% [*Taylor and Nesbitt*, 1998; *Ishizuka et al.*, 2003], ~2% [*Hochstaedter et al.*, 2001], and 0.5 to 2% [*Schmidt*, 2001].

Acknowledgments

[78] The 782A tephra was made available to SMS through the Ocean Drilling Program (College Station/TX). Petra Gloeer and John Longhi are thanked for enduring support with electron microprobe work, W.F. McDonough and I. Horn for enabling the LA-ICPMS analyses at the Harvard lab, and T. Plank and K. Kelley for providing a preliminary Site 1149 bulk sediment composition. Formal journal reviews of C. Bryant, W. White and two anonymous reviewers, as well as the editorial comments of Y. Tatsumi and W. White substantially improved and clarified this paper. This study was funded by the "Deutsche Forschungsgemeinschaft" (grants Str 441/3 and 441/4). The Northeast National Ion Microprobe Facility at WHOI was supported by grants EAR-9628749 and EAR-990440 from the National Science Foundation. This is Lamont Doherty Earth Observatory Contribution 6550.

References

Alves, S., P. Schiano, and C. J. Allegre (1999), Rhenium-osmium isotopic investigation of Java subduction zone lavas, *Earth Planet Sci. Lett.*, *168*, 65–77.

Amma-Miyasaka, M., and M. Nakagawa (2002), Origin of anorthite and olivine megacrysts in island-arc tholeites: Petrological study of 1940 and 1962 ejecta from Miyake-jima volcano, Izu-Mariana arc, *J. Volcanol. Geotherm. Res.*, *117*, 263–283.

Ayers, J. C., S. K. Dittmer, and G. D. Layne (1997), Partitioning of elements between peridotite and H_2O at 2.0–3.0 GPa and 900–1100°C, and application to models of subduction zone processes, *Earth Planet. Sci. Lett.*, *150*, 381–389.

Brenan, J. M., H. F. Shaw, and F. J. Ryerson (1995a), Experimental evidence for the origin of lead enrichment in convergent-margin magmas, *Nature*, *378*, 54–56.

Brenan, J. M., H. F. Shaw, F. J. Ryerson, and D. L. Phinney (1995b), Mineral-aqueous fluid partitioning of trace elements at 900°C and 2.0 GPa: Constraints on the trace element chemistry of mantle and deep crustal fluids, *Geochim. Cosmochim. Acta*, *59*(16), 3331–3350.

Bryant, C. J., R. J. Arculus, and S. M. Eggins (1999), Laser ablation-inductively coupled plasma-mass spectrometry and tephras: A new approach to understanding arc magma genesis, *Geology*, *27*(12), 1119–1122.

Churikova, T., F. Dorendorf, and G. Wörner (2001), Sources and fluids in the mantle wedge below Kamchatka, evidence from across-arc geochemical variation, *J. Petrol.*, *42*(8), 1567–1593.

Class, C., D. M. Miller, S. L. Goldstein, and C. H. Langmuir (2000), Distinguishing melt and fluid subduction components in Umnak volcanics, Aleutian Arc, *Geochem. Geophys.*, *1*, Paper number 1999GC000010.

Donnelly, K. E. (2002), The Genesis of MORB: Extensions and Limitations of the Hot Spot Model, Ph.D. Thesis, Columbia Univ., New York.

Dorendorf, F., U. Wiechert, and G. Wörner (2000), Hydrated sub-arc mantle: A source for the Kluchevskoy volcano, Kamchatka/Russia, *Earth Planet. Sci. Lett.*, *175*, 69–86.

Elliott, T., T. Plank, A. Zindler, W. White, and B. Bourdon (1997), Element transport from subducted slab to juvenile crust at the Mariana arc, *J. Geophys. Res.*, *102*, 14,991–15,019.

Fryer, P., J. A. Pearce, and L. B. Stokking (Eds.) (1992), *Proceedings of the Ocean Drill. Program Scientific Results*, vol. 125, 716 pp., Ocean Drill. Program, College Station, Tex.

Gurenko, A. A., and M. Chaussidon (1997), Boron concentrations and isotopic compositions of the Icelandic mantle: Evidence from glass inclusions in olivine, *Chem. Geol.*, *135*, 21–34.

Hauff, F., K. Hoernle, and A. Schmidt (2003), The Sr-Nd-Pb composition of Mesozoic Pacific oceanic crust (Site 1149 and 801, ODP Leg 185), Implications for alteration of ocean crust and the input into the Izu-Bonin-Mariana subduction system, *Geochem. Geophys. Geosyst.*, *8*(4), 8913, doi:10.1029/2002GC000421.

Hawkesworth, C., S. Turner, D. Peate, F. McDermott, and P. Calsteren (1997), Elemental U and Th variations in island arc rocks: Implications for U-series isotopes, *Chem. Geol.*, *139*, 207–221.

Hickey-Vargas, R. (1998), Geochemical characteristics of oceanic island basalts from the Philippine Sea Plate: Implications of the sources of East Asia plate margins and intraplate basalts, in *Mantle Dynamics and Plate Interactions in East Asia*, *Geodyn. Ser.*, vol. 27, edited by M. J. F. Flower et al., pp. 365–384, AGU, Washington, D.C.

Hilst, R., and T. Seno (1993), Effects of relative plate motion on the deep structure and penetration depth of slabs below the Izu-Bonin and Mariana island arcs, *Earth Planet. Sci. Lett.*, *120*, 395–407.

Hochstaedter, A. F., J. B. Gill, B. Taylor, O. Ishizuka, M. Yuasa, and S. Morita (2000), Across-arc geochemical trends in the Izu-Bonin arc: Constraints on source composition and mantle melting, *J. Geophys. Res.*, *105*, 495–512.

Hochstaedter, A. G., J. B. Gill, R. Peters, P. Broughton, P. Holden, and B. Taylor (2001), Across-arc geochemical trends in the Izu-Bonin arc: Contributions from the subducting slab, *Geochem. Geophys. Geosyst.*, *2*, Paper number 2000GC000105.

Hofmann, A. W. (1988), Chemical differentiation of the Earth: The relationship between mantle, continental crust and oceanic crust, *Earth Planet. Sci. Lett.*, *90*, 297–314.

Horn, I., R. W. Hinton, S. E. Jackson, and H. P. Longerich (1997), Ultra-trace element analysis of NIST SRM 616 and

614 using laser ablation microprobe-inductively coupled plasma mass spectrometry (LAM-ICP-MS): A comparison with secondary ion mass spectrometry (SIMS), *Geostand. Newsl.*, *21*(2), 191–203.

Ishizuka, O., R. N. Taylor, J. A. Milton, and R. W. Nesbitt (2003), Fluid-mantle interaction in an intra-oceanic arc: Constraints from high-precision isotopes, *Earth Planet. Sci. Lett.*, *211*, 221–236.

Janney, P. E., and P. R. Castillo (1997), Geochemistry of Mesozoic Pacific mid-ocean ridge basalt: Constraints on melt generation and the evolution of the Pacific upper mantle, *J. Geophys. Res.*, *102*, 5207–5229.

Jochum, K. P., et al. (2000), New geological standard reference glasses for in-situ microanalysis, *Geostand. Newsl.*, *24*(1), 87–113.

Johnson, M. C., and T. Plank (1999), Dehydration and melting experiments constrain the fate of subducted sediment, *Geochem. Geophys. Geosyst.*, *1*, Paper number 1999GC000014.

Katsumata, M., and L. R. Sykes (1969), Seismicity and tectonics of the Western Pacific: Izu-Mariana-Caroline and Ryukyu-Taiwan Regions, *J. Geophys. Res.*, *74*, 5923–5949.

Kay, R. W., and S. Mahlburg-Kay (1988), Crustal recyling and the Aleutian arc, *Geochim. Cosmochim. Acta*, *52*, 1351–1359.

Kay, S. M., and R. W. Kay (1994), Aleutians magmas in space and time, in *The Geology of Alaska*, edited by G. Plafker and H. C. Berg, pp. 687–722, Geol. Soc. of Am., Boulder, Colo.

Kelley, K. A., T. Plank, J. Ludden, and H. Staudigel (2003), Composition of altered oceanic crust at ODP Sites 801 and 1149, *Geochem. Geophys. Geosyst.*, *4*(6), 8910, doi:10.1029/2002GC000435.

Keppler, H. (1996), Constraints from partitioning experiments on the composition of subduction zone fluids, *Nature*, *380*, 237–240.

Kogiso, T., Y. Tatsumi, and S. Nakano (1997), Trace element transport during dehydration processes in the subducted oceanic crust: 1. Experiments and implications for the origin of ocean basalts, *Earth Planet. Sci. Lett.*, *148*, 193–205.

Langmuir, C. H., R. D. J. Vocke, G. N. Hanson, and S. R. Hart (1978), A general mixing equation wit applications to Icelandic basalts, *Earth Planet. Sci. Lett.*, *37*, 380–392.

Langmuir, C. H., Y. Zhang, B. Taylor, T. Plank, J. Rubenstone, and A. Schmidt (2004), Petrogenesis of Torishima and adjacent volcanoes of the Izu-Bonin arc: One end member of the global spectrum of arc basalts compositions, *Contrib. Mineral. Petrol.*, in press.

Metrich, N., and R. Clochiatti (1989), Melt inclusion investigation of the volatile behavior in historc alkali basaltic magma of Etna, *Bull. Volcanol.*, *51*, 185–198.

Miller, D. M., C. H. Langmuir, S. L. Goldstein, and A. L. Franks (1992), The importance of parental magma composition to calc-alkaline and tholeiitic evolution: Evidence from Umnak Island in the Aleutians, *J. Geophys. Res.*, *97*, 321–343.

Morris, J. D., W. P. Leeman, and F. Tera (1990), The subducted component in island arc lavas: Constraints from Be isotopes and B-Be systematics, *Nature*, *344*, 31–36.

Niu, Y., and Y. Batiza (1997), Trace element evidence from seamounts for recycled oceanic crust in the Eastern Pacific mantle, *Earth Planet. Sci. Lett.*, *148*, 471–483.

Notsu, K., N. Isshiki, and M. Hirano (1983), Comprehensive strontium isotope study of Quaternary volcanic rocks from the Izu-Ogasawara arc, *Geochem. J.*, *17*, 289–302.

Patino, L. C., M. J. Carr, and M. D. Feigenson (2000), Local and regional variation in Central American arc lavas controlled by variations in the subducted sediment input, *Contrib. Mineral. Petrol.*, *138*, 265–283.

Pearce, J. A., and D. W. Peate (1995), Tectonic implications of the compositions of volcanic arc magmas, *Annu. Rev. Earth Planet. Sci.*, *23*, 251–285.

Pearce, J. A., P. D. Kempton, G. M. Nowell, and S. R. Noble (1999), Hf-Nd element and isotope perspective on the nature and provenance of mantle and subduction zone components in Western Pacific arc-basin systems, *J. Petrol.*, *40*(11), 1579–1611.

Pearce, N. J. G., W. T. Perkins, J. A. Westgate, M. P. Gorton, S. E. Jackson, C. R. Neal, and S. P. Chenery (1997), A compilation of new and published major and trace element data for NIST SRM 610 and NIST 612 Glass Reference Material, *Geostand. Newsl.*, *21*(1), 115–144.

Plank, T., and K. Kelley (2001), Contrasting sediment input and output at the Izu and Mariana subduction factories, *Eos Trans. AGU*, *82*(47), Fall Meet. Suppl., F1155.

Plank, T., and C. H. Langmuir (1988), An evaluation of the global variations in the major element chemistry of arc basalts, *Earth Planet. Sci. Lett.*, *90*, 349–370.

Plank, T., and C. H. Langmuir (1993), Tracing trace elements from sediment input to volcanic output at subduction zones, *Nature*, *362*, 739–743.

Plank, T., and C. H. Langmuir (1998), The geochemical composition of subducting sediment and its consequences for the crust and the mantle, *Chem. Geol.*, *145*, 325–394.

Plank, T., J. N. Ludden, and C. Escutia (2000), *Proceedings of the Ocean Drilling, Initial Reports*, vol. 185, Ocean Drill. Program, College Station, Tex.

Prouteau, G., B. Scaillet, M. Pichavant, and R. Maury (1999), Fluid-present melting of ocean crust in subduction zones, *Geology*, *27*(12), 1111–1114.

Ryan, J. G., and C. H. Langmuir (1993), The systematics of boron abundances in young volcanic rocks, *Geochim. Cosmochim. Acta*, *57*, 1489–1498.

Ryan, J. G., L. D. Benton, and I. P. Savov (2001), Isotopic and elemental signatures of the fore-arc, and impacts on subduction recycling: Evidence form the Marianas, *Eos Trans. AGU*, *82*(47), Fall Meet. Suppl., F1275.

Schiano, P., R. Clochiatti, N. Shimizu, R. C. Maury, P. K. Jochum, and A. W. Hofmann (1995), Hydrous silica-rich melts in the sub-arc mantle and their relationship with erupted arc lavas, *Nature*, *377*, 595–600.

Schmidt, A. (2001), Temporal and Spatial Evolution of the Izu Island Arc, Japan, in Terms of Sr-Nd-Pb Isotope Geochemistry, Doctoral Thesis, Christians-Albrecht-Univ., Kiel. (Available at http://e-diss.uni-kiel.de/diss_465/)

Schmidt, A., S. M. Straub, K. A. Hoernle, A. G. Hochstaedter, C. H. Langmuir, and J. B. Gill (1999), Comparative evolu-

tion of the central Izu and Mariana volcanic arcs during the past 15 million years, paper presented at the 22nd General Assembly of the International Union of Geodesy and Geophysics, Birmingham, UK.

Sigmarsson, O., J. Chmeleff, J. Morris, and J. Lopez-Escobar (2002), Origin of ^{226}Ra-^{230}Th disequilibria from southern Chile and implications for magma transfer time, *Earth Planet. Sci. Lett.*, *196*, 189–196.

Sobolev, A. V., A. W. Hofmann, and I. K. Nikogosian (2000), Recycled oceanic crust observed in 'ghost plagioclase' within the source of Mauna Loa lavas, *Nature*, *404*, 986–990.

Stalder, R., S. F. Foley, G. P. Brey, and I. Horn (1998), Mineral-aqueous fluid partioning of trace elements at 900–1200°C and 3.0–5.7 GPa: New experimental data for garnet, clinopyroxene, and rutile, and implications for mantle metasomatism, *Geochim. Cosmochim. Acta*, *62*(10), 1781–1801.

Straub, S. M. (1996), Miocene to Quarternary evolution of the Izu Bonin island arc, *Eos Trans. AGU*, *77*(46), Fall Meet. Suppl., F842.

Straub, S. M. (2002), The evolution of the Izu Bonin - Mariana volcanic arcs (NW Pacific) in terms of major elements, *Geochem. Geophys. Geosyst.*, *4*(2), 1018, doi:10.1029/2002GC000357.

Straub, S. M., and G. D. Layne (2002), The systematics of boron isotopes in Izu arc front volcanic rocks, *Earth Planet. Sci. Lett.*, *198*, 25–39.

Suheyiro, K., N. Takahashi, Y. Ariie, Y. Yokoi, R. Hino, M. Shinohara, T. Kanazawa, N. Hirata, H. Tokuyama, and A. Taira (1996), Continental crust, crustal underplating, and low-Q upper mantle beneath an oceanic island arc, *Science*, *272*, 390–392.

Sun, S. S., and W. F. McDonough (1989), Chemical and isotopic systematics of oceanic basalts: Implications for mantle composition and processes, in *Magmatism in the Ocean Basins*, edited by A. D. Saunders and M. J. Norry, *Geol. Soc. Spec. Publ.*, *42*, 313–345.

Takagi, T., Y. Orihashi, K. Naito, and Y. Watanabe (1999), Petrology of a mantle-derived rhyolite, Hokkaido, Japan, *Chem. Geol.*, *160*, 425–445.

Tamura, Y., and Y. Tatsumi (2002), Remelting of an andesitic crust as a possible origin for rhyolitic magma in oceanic arcs: An example from the Izu-Bonin Arc, *J. Petrol.*, *43*(6), 1029–1047.

Tatsumi, Y., and T. Kosigo (1997), Trace element transport during dehydration processes in the subducted oceanic crust: 2. Origin of chemical and physical characteristics in arc magmatism, *Earth Planet. Sci. Lett.*, *148*, 207–221.

Tatsumi, Y., D. L. Hamilton, and R. W. Nesbitt (1986), Chemical characteristics of fluid phase released from the subducted lithosphere and origin of arc magmas: Evidence from high-pressure experiments and natural rocks, *J. Volcanol. Geotherm. Res.*, *29*, 293–309.

Taylor, B. (1992), Rifting and the volcanic-tectonic evolution of the Izu-Bonin-Mariana Arc, *Proc. Ocean Drill. Program Sci. Results*, *126*, 627–651.

Taylor, R. N., and R. W. Nesbitt (1998), Isotopic characteristics of subduction fluids in an intra-oceanic setting, Izu-Bonin-Arc, Japan, *Earth Planet. Sci. Lett.*, *164*, 79–98.

Turner, S., and J. Foden (2001), U, Th and Ra disequilibria, Sr, Nd and Pb isotope and trace element variations in Sunda arc lavas: Predominance of a subducted sediment component, *Contrib. Mineral. Petrol.*, *142*, 43–57.

Turner, S., F. McDermott, C. Hawkesworth, and P. Kepezhinskas (1998), A U-series study of lavas from Kamchatka and the Aleutians: Constraints on source compositions and melting processes, *Contrib. Mineral. Petrol.*, *133*, 217–234.

Turner, S. P., R. M. M. George, P. J. Evans, C. J. Hawkesworth, and G. F. Zellmer (2000), Time-scales of magma formation, ascent and storage beneath subduction-zone volcanoes, *Philos. R. Trans. Soc. London*, *358*, 1443–1464.

von Huene, R., and D. W. Scholl (1991), Observations at convergent margins concerning sediment subduction, subduction erosion, and the growth of continental crust, *Rev. Geophys.*, *29*, 79–316.

Xu, Y., and S. W. Wise (1992), Middle Eocene to Miocene calcareous nannofossils of Leg 125 from the western Pacific ocean, *Proc. Ocean Drill. Program Sci. Results*, *125*, 43–70.